Cardiac T_1 Mapping: Techniques and Applications

Emily Aherne, MB, BCh, BAO,[1*] Kelvin Chow, PhD,[1,2] and James Carr, MB, BCh, BAO[1]

A key advantage of cardiac magnetic resonance (CMR) imaging over other cardiac imaging modalities is the ability to perform detailed tissue characterization. CMR techniques continue to evolve, with advanced imaging sequences being developed to provide a reproducible, quantitative method of tissue interrogation. The T_1 mapping technique, a pixel-by-pixel method of quantifying T_1 relaxation time of soft tissues, has been shown to be promising for characterization of diseased myocardium in a wide variety of cardiomyopathies. In this review, we describe the basic principles and common techniques for T_1 mapping and its use for native T_1, postcontrast T_1, and extracellular volume mapping. We will review a wide range of clinical applications of the technique that can be used for identification and quantification of myocardial edema, fibrosis, and infiltrative diseases with illustrative clinical examples. In addition, we will explore the current limitations of the technique and describe some areas of ongoing development.

Level of Evidence: 5

Technical Efficacy: Stage 2

J. MAGN. RESON. IMAGING 2020;51:1336–1356.

CARDIOVASCULAR MAGNETIC RESONANCE (CMR) imaging is increasingly used to noninvasively evaluate myocardial structure and function without a need for ionizing radiation. Combining the inherent high soft-tissue contrast of CMR with advanced imaging techniques enables qualitative and quantitative assessment of myocardial composition above and beyond what is currently possible with other noninvasive techniques such as echocardiography and computed tomography (CT). One of the advanced CMR techniques that has demonstrated wide-ranging potential and versatility is myocardial T_1 mapping. It can be used to quantitatively evaluate for the presence of focal or diffuse myocardial disease that can be missed on routine imaging sequences including late gadolinium enhancement (LGE) and conventional T_2-weighted imaging.

LGE has traditionally been considered the clinical standard for evaluation of myocardial scar. Increased accumulation of gadolinium contrast in scar compared with normal myocardium results in focal areas with decreased T_1 relaxation times, which correlate excellently with macroscopic scar on histology.[1] This T_1 difference is visible to the naked eye with T_1-weighted phase-sensitive inversion recovery (PSIR) imaging, and routine clinical practice qualitatively evaluates the presence, extent, and pattern of scarring. However, LGE imaging relies on a region of normal myocardium for reference, and becomes less accurate when the scarring is more diffuse. When this occurs, the absence of normal myocardium for comparison may hinder the visual or even quantitative assessment of scarring.

Myocardial edema results in changes in both T_1 and T_2 relaxation.[1] T_2-weighted imaging, commonly in the form of short-tau inversion recovery (STIR) sequences, are often used clinically to qualitatively assess for edema. However, STIR imaging is susceptible to artifacts from incomplete blood pool suppression, poor breath-holding, and image ghosting from long T_1 fluids including cerebrospinal fluid and pleural effusions.[2] As a weighted technique with qualitative assessment, it is also limited by the general subjectivity of individual readers.

T_1 relaxation time is a physical property that is specific to different tissue compositions and is in part responsible for the high degree of soft-tissue contrast, which is possible on magnetic resonance imaging (MRI). MR T_1 maps can be created that quantify the T_1 relaxation time in each voxel of

View this article online at wileyonlinelibrary.com. DOI: 10.1002/jmri.26866

Received Apr 19, 2019, Accepted for publication Jun 27, 2019.

*Address reprint requests to: E.A.A., Department of Radiology, 676 N. St Clair St., Suite 800, Chicago, IL 60611. E-mail: emily.aherne@gmail.com

From the [1]Department of Radiology, Northwestern University, Chicago, Illinois, USA; and [2]Cardiovascular MR R&D, Siemens Medical Solutions USA, Inc., Chicago, Illinois, USA

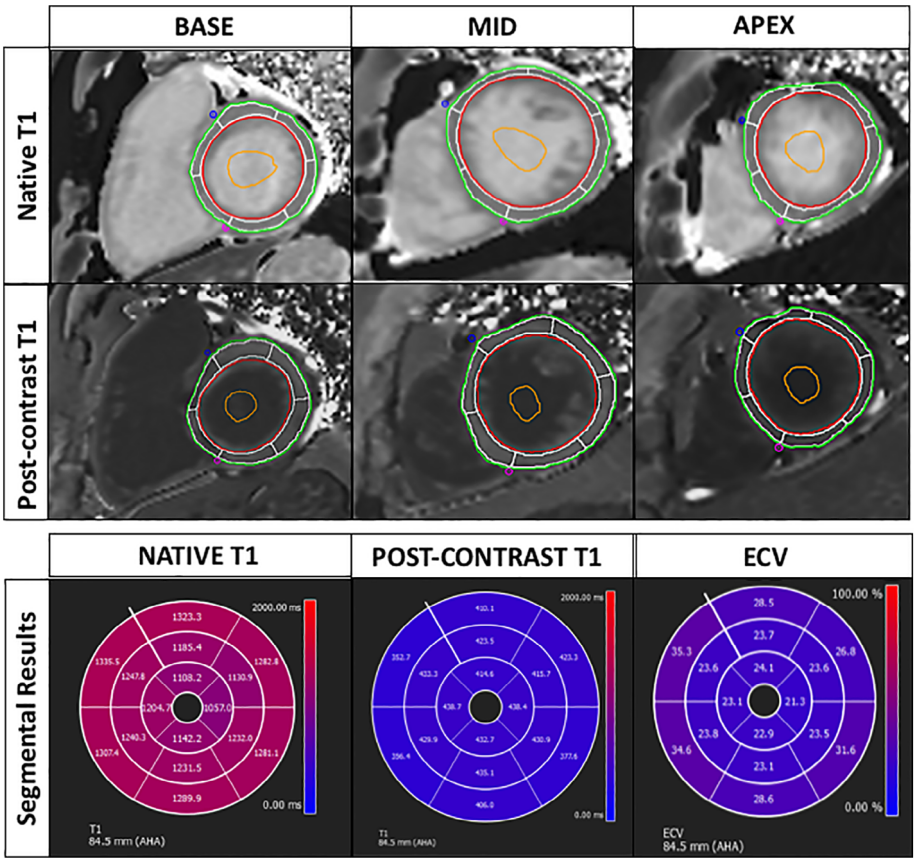

FIGURE 1: Segmental analysis. With dedicated software, it is now possible to analyze the T_1 times of each myocardial segment. An example illustrated here using the Circle cvi42 package. The top two rows illustrate the process of manually segmenting the endocardial and epicardial contours (red and green contours, respectively) of the native and postcontrast maps produced at the time of imaging. It is also possible to produce new maps by entering the raw data. The superior and inferior right ventricular insertion points are also manually marked by the user (blue and pink dots, respectively). This enables the program to produce AHA segmented maps of myocardial native T_1 and postcontrast T_1 times (bottom row, left and middle images). An offset can be used to limit volume averaging at the edges of the myocardium (white). A 10% endo- and epicardial offset was selected in this example. The blood pool is also sampled in each slice (orange). The hematocrit is manually entered. The native and postcontrast maps are then combined, accounting for motion between native and postcontrast acquisitions and segmental ECV maps are produced (bottom right). Data for this, and subsequent clinical examples, are from MyoMaps and prototype sequences.

tissue in the image. Normal myocardium has a predictable T_1 relaxation time but this will be altered in the presence of disease including edema, fibrosis, and infiltrative diseases. T_1 can be used to detect focal or diffuse disease, as well as to evaluate for early, asymptomatic tissue remodeling, not evident on other noninvasive techniques that may be used for risk assessment and prognostication early in disease processes.

We will review the principles of T_1-mapping techniques and their clinical applications in myocardial disease in detail, including a discussion of its limitations and future role.

T_1 Mapping Techniques

Basic Principles

Following RF excitation, protons spin in an MRI system and recover to equilibrium exponentially. The recovery time is characterized by the T_1 value, which is the time for the longitudinal magnetization to recover to 63% of equilibrium following saturation. Conventional T_1 mapping acquires a series of images at various saturation or inversion recovery times and curve fitting is used to calculate the T_1 relaxation time in each voxel of the image. Normal myocardial T_1 times physically vary with magnetic field strength, but measured T_1 values may also vary within specific value ranges that can be defined for individual MR scanners and protocols. With a known normal range of T_1 relaxation times, areas of abnormalities can be quantitatively characterized without the need for a normal myocardial reference on the image. Focal areas of abnormality on other sequences or imaging modalities can be interrogated with targeted region of interest (ROI) analysis or segmental analysis of T_1 maps can be used to systematically evaluate the entire ventricular myocardium (Fig. 1).

Look–Locker Techniques

Numerous techniques have been developed for the purpose of creating T_1 maps. The basis for several popular mapping techniques today was described by Look and Locker in

1970.[3] In this approach, measurements are continuously acquired following an initial inversion pulse, resulting in multiple data points with different inversion times (TIs) that can be fit to an exponential recovery curve.[3] This recovery has a shortened apparent T_1 time, termed T_1*, due to the RF pulses of the imaging readout. However, the true T_1 value can be determined analytically by applying a correction factor, assuming a low flip angle gradient echo readout.[4] This type of acquisition is commonly used as a "TI scout" to determine the optimal null point for LGE imaging and has also been used for cardiac T_1 mapping.[5] The main advantages of this technique include high T_1 map precision due to the large number of measurements and high resolution from the segmented acquisition. However, this method assumes stationary tissue throughout the acquisition and is therefore not ideal for cardiac imaging. Electrocardiographic (ECG) gating can be used to create images throughout the cardiac cycle, but the complex motion does not allow for pixelwise T_1 map calculation and this approach is limited to ROI analysis. Furthermore, through-plane motion can alter the magnetization recovery curve, resulting in T_1 errors.[6]

MOLLI

The MOdified Look-Locker Inversion recovery (MOLLI) sequence was developed to facilitate T_1 mapping while accounting for cardiac motion. Following an inversion pulse, multiple single-shot balanced steady-state free-precession (bSSFP) images are acquired at end-diastole in a number of consecutive cardiac cycles.[7] The TI times of images in this "Look–Locker set" are separated by multiples of the RR interval. Several Look–Locker sets, each with its own inversion pulse, are used in order to better sample the recovery curve with slightly different TIs, with a number of recovery heartbeats between sets to allow for magnetization recovery. The MOLLI sampling scheme is often denoted as a series of numbers indicating the number of images in each Look–Locker set, separated by parenthesized numbers indicating the number of recovery heartbeats.[8] For example, the original MOLLI acquisition scheme is denoted as 3(3)3(3)5, indicating 3 Look–Locker sets, containing 3, 3, and 5 images, respectively, for a total of 11 images. These Look–Locker sets are separated by three recovery heartbeats each, for a total acquisition duration of 17 heartbeats. The acquisition scheme is flexible and MOLLI protocols have been optimized for shorter T_1 times with contrast, reduced heart rate dependence, and shorter breath-holds.

Compared with the conventional continuous Look–Locker approach, MOLLI acquires a reduced number of images, but at the same cardiac phase, thus allowing for pixelwise calculation of T_1 values with motion correction to ameliorate residual cardiac or respiratory motion. Images from all Look–Locker sets are merged into a single dataset and a three-parameter exponential fit is used to calculate the apparent T_1* for each pixel. The true T_1 is estimated by applying the Look–Locker correction factor. MOLLI is the most commonly used technique for cardiac T_1 mapping due to its high signal to noise ratio and good reproducibility when the same pulse parameters are used.[9] However, it is known to underestimate T_1 values due to systematic dependence on T_2 (transverse) relaxation time,[10] magnetization transfer,[11] magnetic field inhomogeneities, off-resonance effects,[12] and inversion pulse efficiency.[13] As a result, MOLLI has high sensitivity to myocardial abnormalities but reduced specificity.

The classic MOLLI technique requires a 17-heartbeat breath-hold, which can be difficult for some patients to perform, particularly those who are acutely unwell or in fluid overload status. A Shortened MOdified Look-Locker Inversion recovery technique (ShMOLLI) was proposed with only nine heartbeats using a 5(1)1(1)1 scheme, following the standardized annotation method described above.[14] Due to the very short, single heartbeat, recovery period between Look-Locker sets, conditional data analysis is applied wherein data from the last two Look–Locker sets are only included if the T_1 is so short as to allow near-complete recovery between Look–Locker sets. Another commonly used technique with reduced breath-hold duration is the 5(3)3 MOLLI protocol (Fig. 2a,c), which acquires the longest Look–Locker set at the beginning, reducing heart rate dependent errors compared with the classic MOLLI protocol.

Saturation Recovery Techniques

The prototype SAturation recovery single-SHot Acquisition (SASHA) sequence[15] consists of 10 ECG-gated single-shot bSSFP images acquired in consecutive heartbeats (Fig. 2b). No magnetization preparation is applied prior to the first image and the remaining nine images are acquired following nine respective saturation pulses with variable saturation recovery times (Fig. 2d). Unlike the MOLLI family of sequences, each saturation pulse resets the magnetization to zero, and thus each image is independent of each other. As a result, SASHA and other saturation recovery T_1 mapping sequences like SMART1Map, SAP-T1, and SR-TFL[16–18] are more accurate, and not susceptible to bias from T_1, T_2, magnetization transfer, or magnetic field heterogeneities.[8,11,12,19,20] However, the reduced dynamic range of saturation recovery compared with inversion recovery (IR) results in generally reduced T_1 precision compared with IR sequences such as MOLLI.[15] Recent work using a variable flip angle readout combined with a two-parameter fit[21] and optimization of saturation recovery times[22] have improved the myocardial T_1 precision of SASHA to be similar to MOLLI.[23]

A combined SAturation Pulse Prepared Heart rate-independent Inversion REcovery (SAPPHIRE) sequence has also been proposed to combine the independent image properties of saturation recovery approaches and the higher dynamic range of inversion recovery.[24] The SAPPHIRE technique

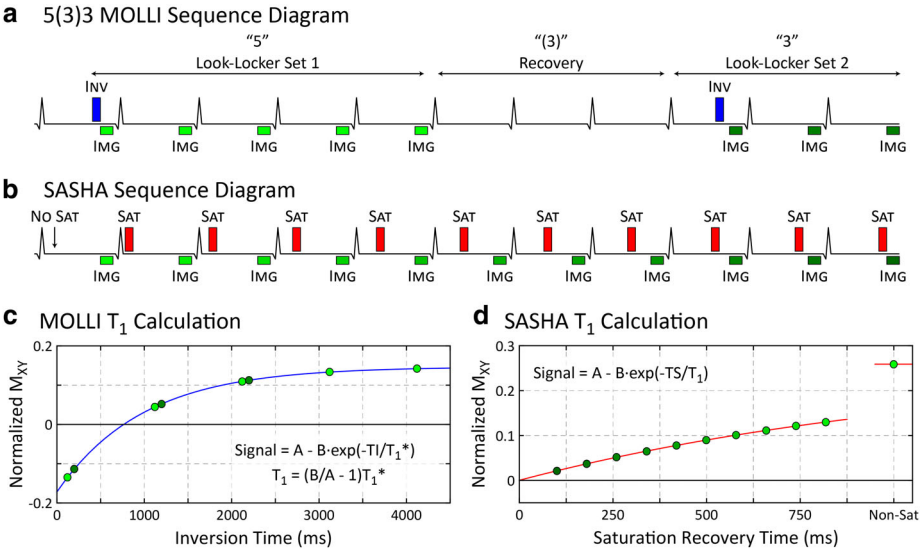

FIGURE 2: MOLLI and SASHA T_1 mapping techniques a: Pulse sequence diagram for a 5(3)3 MOLLI scheme commonly used for native T_1 mapping. b: Pulse sequence diagram for an 11 heartbeat SASHA sequence with variable saturation recovery times. c: Calculation of MOLLI T_1 values utilizing a "Look-Locker correction factor" to estimate the true T_1 value. d: Calculation of SASHA T_1 using a three-parameter recovery model.

produced similar T_1 values to SASHA with precision in between MOLLI and the original three-parameter SASHA.

Recent Advancements

Motivated by a clinical desire for greater spatial coverage and intrinsic higher signal-to-noise, there has been renewed interest in 3D techniques.[25–27] These techniques may allow for characterization of the thin, complex structure of the right ventricle (RV) or atria that have been difficult to image with existing techniques. Another approach for increased spatial coverage is the multislice "Slice-interleaved T_1" (STONE) technique, which employs a "MOLLI-like" acquisition with five images being acquired after a single inversion pulse. However, as five images are acquired in different slices, the myocardial signal in each slice is unaffected by the previous imaging readouts. This pattern is repeated several times in free-breathing with different slice ordering, such that the IR curve is well sampled for each slice. The free-breathing multislice nature of STONE is appealing, but is limited by the inability to accurately quantify blood pool T_1 values due to blood flow between slices during the acquisition.

The SASHA technique has also been extended to a free-breathing acquisition using a modified image readout to produce images with high blood-tissue contrast needed for robust image registration.[28] The sequence repeats a basic SASHA acquisition with optimized saturation recovery times and a subset of images at a similar respiratory phase are selected and motion-corrected. Free-breathing SASHA had similar myocardial T_1 values to the original SASHA technique, with a myocardial T_1 precision similar to MOLLI, with ~30 seconds of free-breathing. However, the technique has not been extensively validated in long-axis slice orientations where retrospective motion correction may be more challenging.

Native T_1, Postcontrast T_1, and Extracellular Volume (ECV): Acquisition and Calculation

Normal myocardium is composed of three major compartments: intracellular, intravascular, and interstitial. The intracellular compartment is the largest of the three in normal myocardium and consists predominantly of myocytes, but also includes fibroblasts, endothelial cells, and smooth muscle cells. The intravascular compartment contains the blood, while the interstitial compartment provides a structural support network around the myocytes to maintain tissue architecture and to transmit mechanical forces. In normal myocardium, it is composed of fibrillary collagen, proteogylcans, and other signaling molecules. Together, the interstitial and intravascular compartments are often referred to as the ECV. In the majority of cardiovascular diseases such as extracellular edema or interstitial, replacement, or infiltrative fibrosis, the ECV becomes expanded, primarily due to expansion of the interstitial component.

Native T_1 mapping refers to the acquisition of T_1 maps without the use of contrast agents. Changes in the relative sizes of the intracellular and ECV alter the T_1 relaxation time of the myocardium. In edema and other fibrotic conditions, expansion of the extracellular space where water is less restricted in motion results in an increase of native T_1 values. For infiltrative diseases such as Anderson–Fabry and iron overload, extracellular accumulation of short T_1 lipids and iron respectively result in decreased native T_1 values. Native T_1 mapping is clinically appealing, as contrast agents are not required; however, the relatively small changes in native T_1 values with most cardiomyopathies can be difficult to detect. Additionally, changes in native T_1 values are not specific to changes in the ECV and normal absolute T_1 values may vary with magnetic field strength and T_1 mapping technique.

Standard gadolinium-based contrast agents are distributed throughout the extracellular space and decrease the T_1 time of these tissues relative to the extracellular volume (Fig. 3). The absolute contrast-enhanced myocardial T_1 values are variable and depend on factors including the administered dose, time postinjection, renal function, and anemia.[29] The contrast concentration in the myocardium can be estimated using the native and postcontrast T_1 values, and normalized to the blood concentration to yield the blood-tissue partition coefficient, λ:

$$\lambda = \frac{1/T_{1\,(tissue\ post-Gd)} - 1/T_{1\,(tissue\ native)}}{1/T_{1\,(blood\ post-Gd)} - 1/T_{1\,(blood\ native)}}$$

The partition coefficient can be further corrected for the distribution of contrast agent within the blood pool itself to estimate the ECV:

$$ECV = (1 - hematocrit)\frac{1/T_{1\,(tissue\ post-Gd)} - 1/T_{1\,(tissue\ native)}}{1/T_{1\,(blood\ post-Gd)} - 1/T_{1\,(blood\ native)}}$$

For accurate ECV estimates, postcontrast measurements should be performed >10 minutes after contrast administration to allow for a dynamic equilibrium between blood and tissue.[30] Unlike postcontrast T_1 mapping values, ECV values are reproducible[19,31,32] and there is high agreement between ECV and histologically proven myocardial collagen content.[33,34] While ECV has reduced sensitivity to T_1 measurement errors, systematic biases in ECV values between different sequences[19] may occur. Additionally, errors in any of the five measurements propagate to the ECV itself, leading to lower precision than a single native T_1 measurement.

Synthetic Hematocrit

ECV measurements require the use of hematocrit to account for the distribution of contrast agent within the blood pool. However, in clinical environments the hematocrit may not be available at the time of the CMR exam. Using the well-established relationship between blood T_1 values and hematocrit, a prototype "synthetic" hematocrit value can be calculated using native blood T_1 measurements,[35] allowing for the possibility of MR-only estimates of ECV. However, only a moderate relationship (R2 = 0.45–0.51) exists between T_1 and hematocrit and the relationship must be calibrated for the each individual T_1 mapping technique.

Normal Ranges

Interpretation of any quantitative diagnostic test requires a normal reference range for comparison and this has been a major limitation for the integration of T_1 mapping into mainstream clinical use. Several groups have attempted to provide a range of normal values, but a range exists depending on the magnet strength and protocol used (Table 1).[14,36–40] Development of the normal range has been challenging for native T_1 and ECV

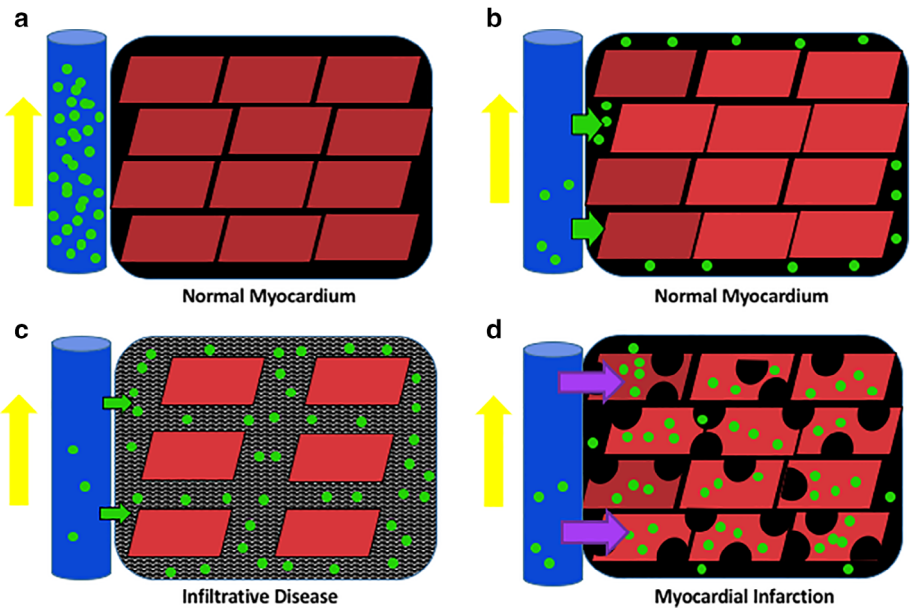

FIGURE 3: Gadolinium distribution in normal myocardium and disease. Schematic representing distribution of gadolinium postinjection in normal myocardium (a,b), in the setting of infiltration/fibrosis (c) and in the setting of acute infarction (d). a: Postinjection gadolinium chelates are distributed into the capillary bed. b: From the capillary bed they diffuse into the interstitial space but cannot cross through myocyte cell membrane, as gadolinium is an extracellular contrast agent. In normal myocardium the myocytes are closely packed together with a small volume of surrounding interstitial space and so only a little gadolinium accumulates. c: In the setting of infiltrative disease, and to a lesser extent fibrosis, the interstitial compartment increases in size and this results in increased volume of accumulated gadolinium chelates within the interstitium, resulting in hyperenhancement in T_1-weighted images due to shortening of the T_1 time of myocardium. d: In the setting of myocardial enhancement, breakdown of the cellular membrane allows gadolinium chelates to diffuse into the intracellular space which also results in hyperenhancement.

TABLE 1. Overview of Larger Studies Reporting Normal Values for Native T1 Mapping and ECV

Sequence	Magnet strength	Participants	Native T1 (msec)	Participants	Contrast (mmol/kg)	ECV (%)	Author (Reference)	Year
MOLLI 3(3)3(3)5	1.5T	34: healthy volunteers	950 ± 21	34: healthy volunteers	0.1–0.2	25 ± 4	Dabir et al [36]	2014
		58: low-risk patients	952 ± 23	58: low-risk patients		26 ± 6		
MOLLI 3(3)3(3)5	1.5T	84: healthy volunteers	944 ± 25	37: healthy volunteers	0.15	25 ± 2	Rauhalammi et al [37]	2016
MOLLI 5(3)3 native/4(1)3(1)2 post	1.5T	94: healthy volunteers	1024 ± 39	94: healthy volunteers	0.1	27 ± 3	Rosmini et al [38]	2018
MOLLI 5(3)3 native/4(1)3(1)2 post	1.5T	101: healthy volunteers	1013 ± 27				Bulluck et al [39]	2017
ShMOLLI	1.5T	374: healthy volunteers	962 ± 25				Piechnik et al [14]	2013
ShMOLLI	1.5T	94: healthy volunteers	957 ± 30	94: healthy volunteers	0.1	30 ± 3	Rosmini et al [38]	2018
SASHA	1.5T	94: healthy volunteers	1144 ± 45	94: healthy volunteers	0.1	24 ± 3	Rosmini et al [38]	2018
MOLLI 3(3)3(3)5	3T	32: healthy volunteers	1052 ± 23	32: healthy volunteers	0.1–0.2	26 ± 4	Dabir et al [36]	2014
		55: low-risk patients	1053 ± 24	55: low-risk patients		26 ± 6		
MOLLI 3(3)3(3)5	3T	84: healthy volunteers	1155 ± 26				Rauhalammi et al [37]	2016
ShMOLLI	3T	57: healthy volunteers	1125 ± 45		0.2	25 ± 3	Costello et al [40]	2017
SASHA	3T	57: healthy volunteers	1494 ± 43		0.2	20 ± 2	Costello et al [40]	2017

values due partly to the large number of T_1 mapping techniques available without standardization of how techniques are validated, compared, and reported in the literature. As T_1 values from techniques such as MOLLI may be sensitive to implementation, specific parameters such as sampling scheme, flip angle, and inversion pulse design, normal values may not generalize beyond a specific protocol. Normal T_1 values also vary with magnetic field strength, where native T_1 values are higher at 3T compared with 1.5T. The location of T_1 measurement may also affect the expected normal values, as higher values at the apex compared with the base and mid-ventricle are likely related to more pronounced partial volume averaging effect at the apex. Lower values at the lateral wall compared with the septum may be related to off-resonance effects and reduced signal to noise ratio in the region as it is farthest away from the coil.[41] Female sex appears to be associated with marginally increased native T_1 and ECV values.[36,38,39,42–44] The effect of age on normal native T_1 and ECV values is unclear, as studies have shown conflicting results with decreased values, increased values, or no effect reported.[36,42,45,46]

Clinical Applications

Utilization of CMR for the diagnostic and prognostic evaluation of a wide variety of cardiac disorders is of significant interest and is increasing over time. As well as accurately quantifying cardiac morphology and function, its primary clinical value is in noninvasive tissue characterization. Native T_1 mapping and ECV have a significant role to play in both the diagnostic workup and prognostication of a wide variety of cardiac disorders.

Edema

Myocardial edema is associated with almost any acute myocardial injury. It results in increased myocardial native T_1 and T_2 values. Since it is easier for the eye to perceive the signal changes on T_2-weighted imaging, this was initially pursued as the method of choice for identification of edema. It has since been shown that native T_1 mapping is superior to both conventional T_2-weighted imaging and LGE in the identification of acute myocardial inflammation.[47–49] More recently, T_2 mapping has also been employed for quantitative assessment of myocardial edema and allows identification of ischemic segments vs. remote myocardium.[50] T_1 and T_2 mapping techniques are both sensitive to the presence of edema and the T_1 and T_2 times are directly related in their response to the presence of edema. Similar to T_2 mapping, T_1 mapping also allows for quantitative evaluation of the presence of edema and has been shown to have a high diagnostic accuracy when compared with conventional T_2-weighted imaging.[51] In animal studies, it has been shown that T_1 mapping is even more accurate in identification of myocardial edema than T_2 mapping when compared with histologic specimens.[52] Given the ever-present time constraints with clinical MRI, in the correct clinical setting it is possible that native T_1 mapping could be used in lieu of T_2 mapping with high diagnostic accuracy for the detection and quantification of myocardial edema.

ACUTE MYOCARDITIS (FIG. 4). Acute myocarditis can be a difficult condition to diagnose clinically. It is most commonly caused by a viral infection but can also be caused by bacterial, fungal, or parasitic infection and has a number of noninfectious causes, including drug effects such as chemotherapy agents and recreational drugs, prior radiation, prior transplant, or associated with acute phases of systemic inflammatory conditions including systemic lupus erythematous, sarcoidosis, and rheumatoid arthritis.[53–55] It has a variable clinical presentation that ranges through a wide spectrum from asymptomatic to cardiogenic shock and sudden death. Viral myocarditis is usually associated with a viral prodrome including fever but symptoms and laboratory tests are often nonspecific. We know that persistent myocardial inflammation is associated with poor clinical outcome, including progression to dilated cardiomyopathy.[56] Although endomyocardial biopsy is the gold standard for diagnosis, it is not frequently performed for a variety of reasons, including the low diagnostic yield, associated serious risks of the procedure including perforation and tamponade, as well as limited access and availability.[57,58] In recognition of CMR as the current primary diagnostic tool for the assessment of suspected acute myocarditis, the CMR-based imaging Lake Louise consensus criteria were developed in 2009.[59] Initially, the criteria were based on imaging findings seen on conventional T_2-weighted sequences, early gadolinium enhancement pattern and LGE and several studies have shown that it is extremely useful for assessment in both the diagnosis and recovery of patients with myocarditis without the need for contrast administration.[47,60,61] Although LGE can persist in those with decreasing inflammation, native T_1 mapping normalizes as the myocardium recovers and can differentiate between those with active inflammation vs. healed disease.[60] In 2018, the Lake Louise criteria were updated to include parametric mapping techniques including T_1 and T_2 mapping and ECV.[62]

ACUTE MYOCARDIAL INFARCT. Another very common etiology for myocardial edema in clinical practice is acute myocardial infarction. Coronary vascular occlusion, most commonly caused by a ruptured atherosclerotic plaque or occlusive embolus, leads to myocardial ischemia and apoptosis at a cellular level. In animal models, edema has been shown to be a very early marker of ischemia that can be seen on T_2-weighted MRI as hyperintense signal within 28 ± 4 minutes postonset of ischemia,[63] which could theoretically facilitate early diagnosis. LGE is a well-established technique used for the evaluation of the presence and extent of myocardial

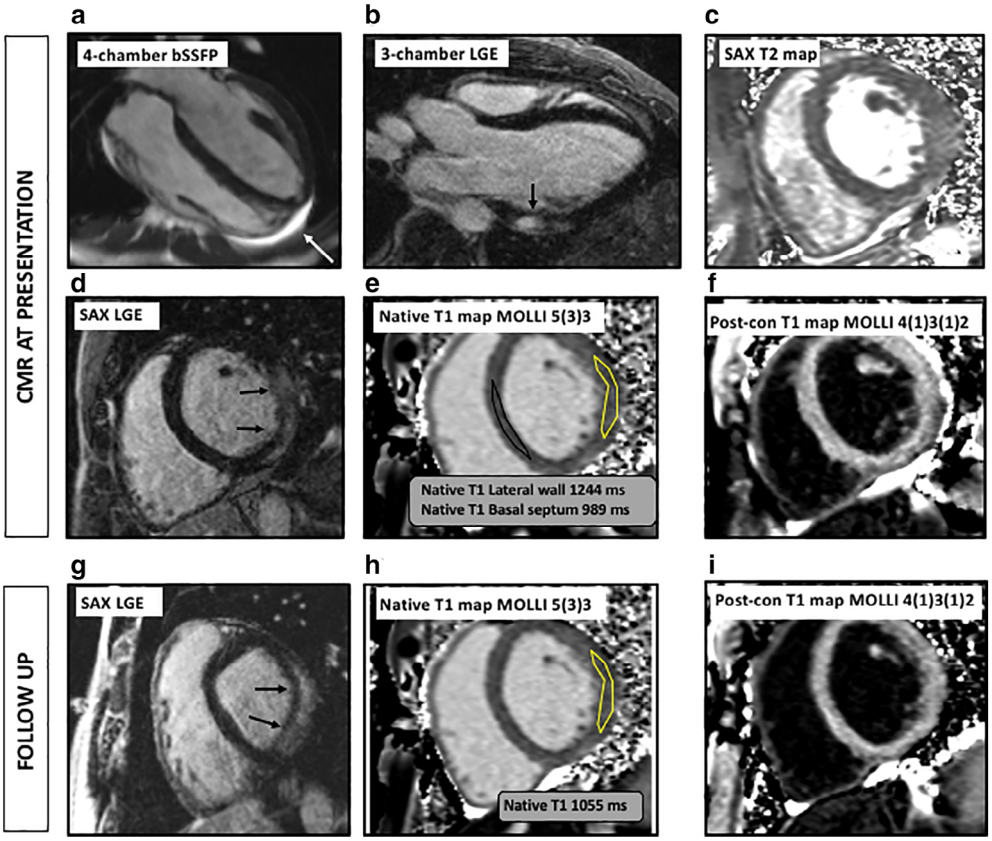

FIGURE 4: Acute myopericarditis with follow-up. A 21-year-old male patient admitted with intermittent chest pain for 1 week following an upper respiratory tract infection. On admission, troponin was elevated at 3.13 ng/mL. a: Axial bSSFP image shows a small pericardial effusion (white arrow). b: Three-chamber postcontrast image shows focal mesocardial to epicardial delayed gadolinium enhancement in the basal lateral wall (black arrow) consistent with myocarditis. c: There is elevated T_2 time in this region (59 msec) compatible with edema. d: Short axis view of delayed gadolinium uptake in the basal lateral wall (black arrows). e: Elevated native T_1 time in the region of edema of 1244 msec. Normal T_1 time in the basal septum of 989 msec. f: Postcontrast T_1 map allows calculation of ECV of 29% compared with 23% in the basal septum. g: Follow-up CMR 8 weeks later shows similar to slightly increased uptake of gadolinium in the basal lateral wall (black arrows). h,i: The native T_1 time has decreased to 1055 msec and the ECV was decreased to 23%, compared with 22% in the basal septum. These findings suggest that the acute inflammation decreased although the scar continued to evolve.

infarction and in the identification and quantification of viable myocardium prior to revascularization procedures. We have known for some time that T_1 maps can detect infarcted myocardium[64] but it has also recently been shown that the T_1 values may be used to evaluate for viable myocardium without the need for contrast administration.[65] Presently, CMR is infrequently performed as part of a workup for acute myocardial infarct due to the time required in most centers for coordination, acquisition, and interpretation of images and it is not part of the standard algorithm for evaluation of acute myocardial infarct.

STRESS-INDUCED CARDIOMYOPATHY (FIG. 5). Stress-induced (takotsubo) cardiomyopathy is an acute heart failure syndrome usually precipitated by an intense emotional event and it is classically associated with a rapid recovery. In the acute stage, native T_1 mapping can be used to identify the known associated acute myocardial edema.[51] More recently, it has also been shown that this form of cardiomyopathy is likely associated with longer-lasting sequelae than was previously assumed and that native T_1 values remain persistently elevated 13–39 months after the initial event.[66]

ACUTE CARDIAC ALLOGRAFT REJECTION POSTTRANSPLANTATION. Traditionally, patients postcardiac transplantation are evaluated with serial endomyocardial biopsies to monitor for acute allograft rejection, which is the leading cause of death in the first year posttransplant.[67] Endomyocardial biopsy is an invasive procedure and it does not provide information on cardiac structure or function. CMR has been proposed as a noninvasive alternative. Recent studies have shown that a combination of T_2 mapping and ECV have the potential to be used as a surrogate biomarker for rejection.[68,69] Additionally, ECV values are elevated in the myocardium of patients with multiple rejection episodes and may point to a poorer prognosis. However, larger studies will be required for validation.

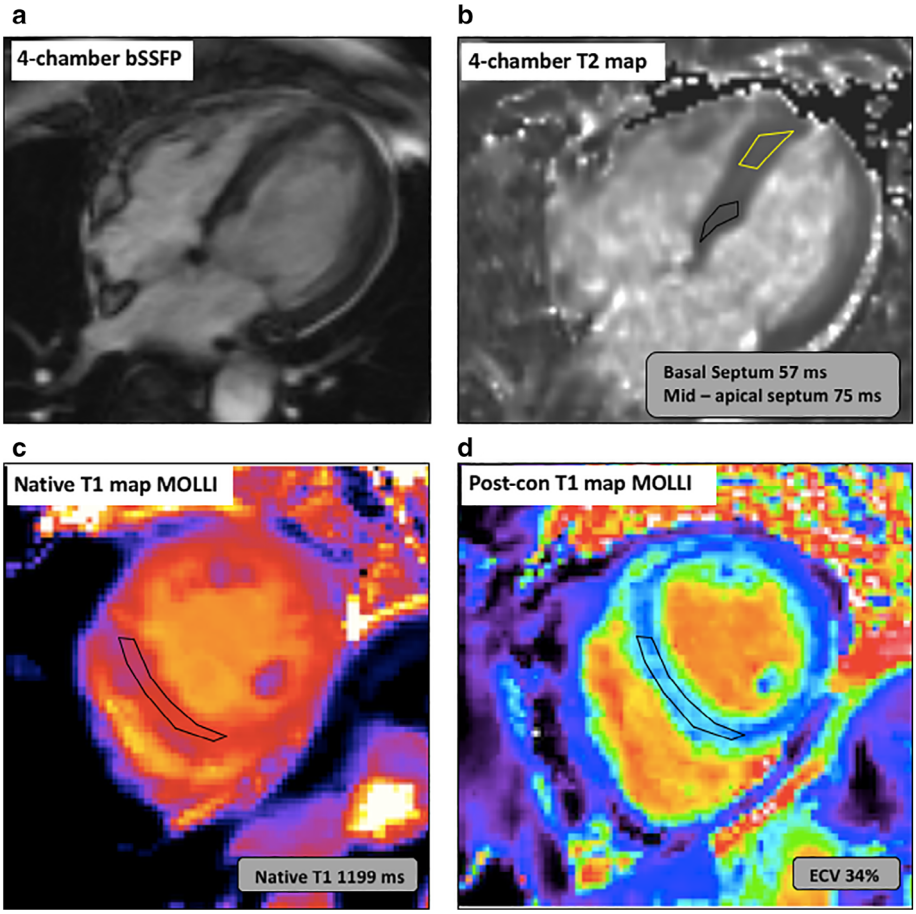

FIGURE 5: Stress-induced (Takotsubo) cardiomyopathy. A 73-year-old previously healthy patient collapsed while walking into a community center, witnessed by a bystander. She had no recollection of the preceding moments but did fracture her jaw during the fall. On admission to the emergency department, her troponin was elevated and her ECG was abnormal. Echocardiogram showed severe hypokinesis of the apical regions. Given the distribution of these findings and a normal coronary angiogram 1 year prior, acute stress associated cardiomyopathy was suspected. CMR was performed. a: Four-chamber bSSFP imaging showed a mildly dilated left ventricle with apical hypokinesis. b: There was elevated T_2 times throughout the left ventricle but most pronounced from the mid to apex. c,d: Markedly elevated native T_1 (1199 msec) and ECV (34%) values in the mid to apex in keeping with extensive edema in a pattern in keeping with acute stress-induced cardiomyopathy. Follow-up sequential echocardiograms demonstrated eventual resolution of wall motion abnormalities. Stress echocardiogram performed 15 months later showed no evidence of exercise-induced ischemia.

Fibrosis

Histologically, myocardial fibrosis is characterized by increased collagen in the interstitial compartment of the myocardium. Fibrosis can be focal, such as related to a discrete chronic myocardial infarct, or diffuse, such as is seen in cardiomyopathies.

CHRONIC ISCHEMIC SCAR. It has been known for some time that chronically infarcted myocardium has an increased native T_1 value which is higher than remote myocardium but not as high as an acute infarct.[64] In a recent study including 30 patients with acute ST-elevation myocardial infarct (MI), 30 patients with an infarct for more than 1 year and 20 control patients, native T_1 mapping was able to differentiate between viable and nonviable myocardium in patients with chronic MI with a sensitivity and specificity of 88% and 88%, respectively. The technique performed better in chronic infarction compared with acute infarction (sensitivity and specificity of 79% and 79%) due to the absence of edema that can confound the values.[65]

DILATED CARDIOMYOPATHY. Dilated cardiomyopathy (DCM) is increasing recognized as a cause of significant morbidity and mortality. Diffuse remodeling of the myocardium is a sequela of a variety of underlying etiologies that occurs by complex processes including extracellular matrix remodeling, myofibroblast transformation, and cardiomyocyte cell loss leading to interstitial fibrosis.[70,71] LGE is routinely used to identify the presence and distribution of macroscopic scar, the pattern of which may indicate an underlying disease etiology. It has also been shown that in patients with nonischemic DCM the identification of LGE is associated with increased risk of all-cause mortality, hospitalization, heart transplant, and sudden cardiac death.[72] Increased values on

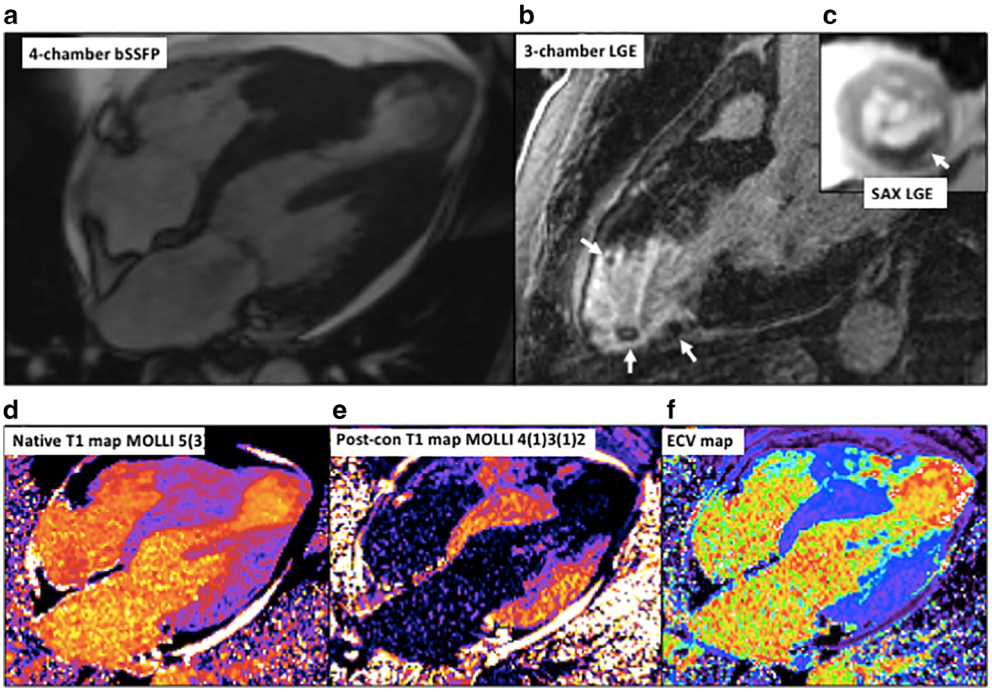

FIGURE 6: Apical hypertrophic cardiomyopathy. A 74-year-old male patient with known apical variant hypertrophic cardiomyopathy who underwent CMR after transient ischemic attack causing visual disturbance to evaluate for intracavity thrombus. The patient had ceased anticoagulation 2 months prior. a: Four-chamber bSSFP imaging shows typical configuration of advanced apical variant HCM with formation of an apical aneurysm. b: On two-chamber LGE imaging, multiple small foci of thrombus are noted within the aneurysm (arrows). c: A large focus of submural thrombus is confirmed on short axis LGE imaging through the apex (arrows). d: Native T_1 values were mildly increased throughout the myocardium consistent with diffuse fibrosis (1054 msec). e: Postcontrast T_1 map. f: ECV was also diffusely mildly elevated (30%).

native T_1 mapping and ECV can identify the presence of diffuse scar within the myocardium and can differentiate between normal tissue and fibrosis.[73,74] Furthermore, recently it has also been shown that T_1 mapping is an independent predictor of outcomes in nonischemic DCM including all-cause mortality, heart failure-associated hospitalizations, and death and heart transplant.[75,76] This suggests it is a useful technique to noninvasively guide risk stratification and management of these patients.

HYPERTROPHIC CARDIOMYOPATHY (FIG. 6). Hypertrophic cardiomyopathy (HCM) is an autosomal dominant genetic condition that results in regions of abnormal myocardial hypertrophy in various patterns.[77] Histologically, there is underlying myocyte hypertrophy and disarray, with expansion of the interstitial compartment.[78] More focal regions of fibrosis can be typically seen on LGE as patchy areas of enhancement in hypertrophied segments and at the RV insertion points.[79] However, histologically HCM appears to be a much more diffuse process which is not always apparent on LGE. Native T_1 values are increased in HCM.[73,80,81] Increased T_1 values correlate positively with wall thickness,[80] which suggests that it can be used as a marker of disease severity. ECV values are also increased in HCM and have been shown to be significantly more increased compared with those with hypertensive heart disease, a common differential in earlier stages.[81] However, in that study, native T_1 was a better independent discriminator between HCM and hypertension-associated myocardial hypertrophy than ECV, wall thickness, or indexed left ventricular (LV) mass.

It is also possible to utilize T_1 mapping to help distinguish between HCM and LV hypertrophy seen in healthy athletes, a difficult clinical dilemma due to the devastating impact of an HCM diagnosis on an athletic career. In athletic LV hypertrophy, it is the volume of cardiomyocytes and therefore the intracellular compartment that predominantly increases, causing a decrease in ECV values. In patients with HCM there is infiltration of the interstitial compartment in the extracellular compartment as well as myocyte hypertrophy, which leads to increased ECV.[82]

NONCOMPACTION CARDIOMYOPATHY. Noncompaction of the LV is a genetic condition that develops due to a premature arrest of myocardial compaction during embryogenesis. There are resultant prominent LV trabeculations, usually most prominent at the ventricular apex, with deep intervening recesses that communicate with the ventricle. Several different subtypes exist including dilated, hypertrophic, mixed dilated, and hypertrophic and restrictive.[83] The RV can also be involved, although this is not seen in all cases. It is a

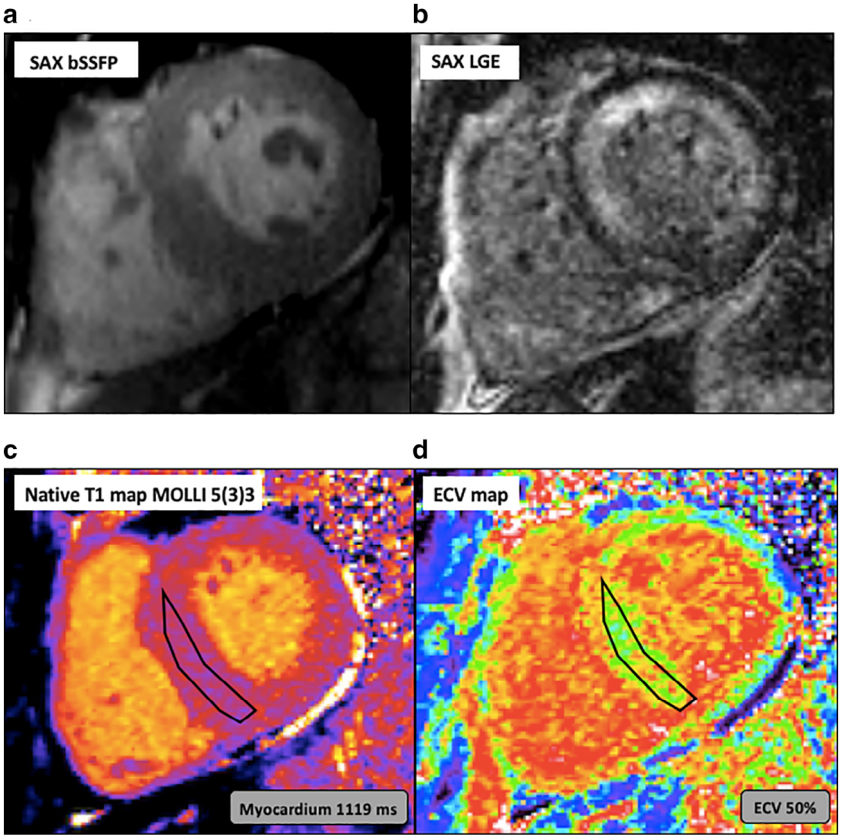

FIGURE 7: Amyloidosis. A 61-year-old male patient with IgG lambda monoclonal plasma cell dycrasia on biweekly carfilzomab and methylprednisone infusions. Left ventricular hypertrophy was seen on echocardiogram. CMR was performed. a: Short axis bSSFP imaging confirms concentric left ventricular hypertrophy. b: Short axis late gadolinium enhanced image demonstrates extensive patchy mesocardial and subendocardial enhancement in a pattern suspicious for amyloidosis. c: Native T_1 maps shows elevated T_1 times of 1119 msec. d: Postcontrast T_1 map and hematocrit allows calculation of severely elevated ECV of 50%. Overall, these findings are consistent with amyloidosis.

relatively rare disease that is often identified at a late stage. It is associated with arrhythmias, heart failure, and formation of ventricular thrombus.[83] It can also be seen in conjunction with congenital heart disease. A small study including 31 patients and 8 controls showed that T_1 values are elevated in those with noncompaction cardiomyopathy compared with normal controls, even in those without LGE. This suggests that it may be more sensitive for the detection of fibrosis in these patients than LGE.[84] Larger studies would be required to validate this finding but difficult to perform due to the rarity of the condition.

HEART FAILURE WITH PRESERVED EJECTION FRACTION. Heart failure with preserved ejection fraction (HFpEF) accounts for a significant fraction of all of those with heart failure, and although survival rates are slightly better in this group compared with those with systolic heart failure, they do not improve over time.[85] Increased LV stiffness leads to slow LV relaxation in diastole and resultant elevated diastolic filling pressures limit cardiac performance both at rest and during exercise.[86,87] Both increased interstitial fibrosis and cardiomyocyte stiffness contribute to diastolic dysfunction.[88] Supporting this paradigm, it has been demonstrated that ECV is increased in patients with HFpEF compared with patients without heart failure.[89]

Infiltrative Disorders

T_1 mapping is an important tool in the diagnosis of infiltrative diseases. In these diseases, abnormal proteins accumulate within the interstitial tissues and alter the T_1 properties of the interstitial compartment, most floridly seen with amyloidosis. Some diseases are associated with increased native T_1 values including amyloidosis, sarcoidosis, and systemic sclerosis. Others are associated with decreased myocardial native T_1 values, including iron deposition and Anderson–Fabry disease.

AMYLOIDOSIS (FIG. 7). The characteristic diffuse infiltration of the interstitial compartment by pathologic amyloid proteins and a resultant increase accumulation of gadolinium on LGE results in patchy or diffuse myocardial enhancement. Unfortunately, the diffuse infiltration alters the signal characteristics of the myocardium so much that there are often significant difficulties with nulling of the myocardium in order to allow optimal evaluation of LGE.[90,91] Patients with

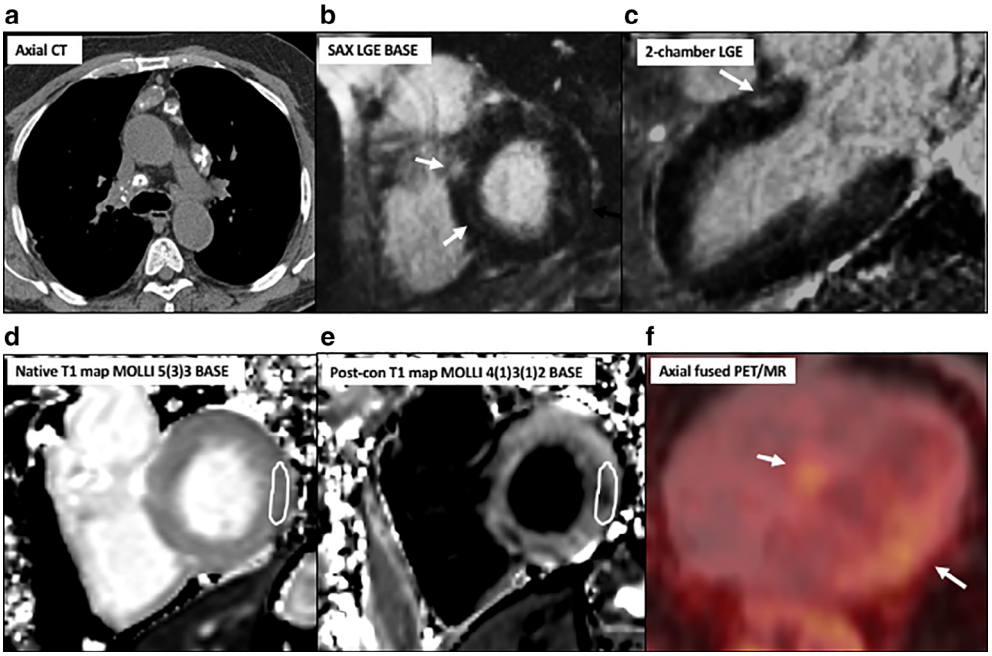

FIGURE 8: Sarcoidosis. A 74-year-old male with multisystemic sarcoidosis for more that 40 years involving the lungs, lymph nodes, heart, conjunctiva, skin, and joints. CT studies showed progression of pulmonary disease and CMR was requested to evaluate for active cardiac sarcoidosis. a: Axial CT through the upper thorax demonstrates calcified mediastinal adenopathy consistent with longstanding sarcoidosis. b,d: Axial and two-chamber LGE imaging demonstrate small patchy areas of mesocardial and epicardial enhancement, most prominent at the base (arrows). d,e: Native and postcontrast T_1 maps demonstrate increased native T_1 and ECV in the regions of infiltration (for example, 1243 msec and 33% respectively in the lateral wall). f: Patchy areas of increased FDG uptake seen in the basal septum and lateral wall (arrows) are compatible with active cardiac sarcoidosis.

amyloidosis also often have renal failure as a manifestation of the disease and contrast-enhanced imaging is not always possible. It has been demonstrated that in both light chain and transerythretin type amyloidosis the native T_1 values are markedly elevated above normal values,[92,93] which allows for a high diagnostic accuracy. Native T_1 values are elevated in both types of amyloidosis but more so in the light chain type than the transerythretin type. In patients who can receive gadolinium contrast, the ECV is frequently high (>35–40%) and suggests a high suspicion for a cardiac amyloid diagnosis.

SARCOIDOSIS (FIG. 8). Sarcoidosis is a noncaseating, granulomatous infiltrative disease, which most commonly affects the lungs and hilar lymph nodes but can involve many different organs. Clinically, cardiac sarcoidosis is diagnosed only in a small percentage of these patients, but it is much more commonly evident at the time of postmortem,[94] which suggests that it is underdiagnosed. Cardiac sarcoidosis is associated with significant morbidity and mortality causing arrhythmias, heart failure, and sudden death. It has recently been shown that in patients with biopsy-proven systemic sarcoidosis, myocardial T_1 values were significantly higher at baseline than normal controls and also that native T_1 values provided excellent discrimination between normal controls and those with disease (area under the curve [AUC] = 0.96).[95] Elevated T_1 values were noted even in those who were asymptomatic, which suggests that T_1 mapping may allow early recognition of cardiac involvement in this condition. Furthermore, in patients who received systemic steroids the T_1 values decreased on follow-up MRI compared with no change in those who had not received treatment,[95] possibly related to a reduction in myocardial inflammation.

AUTOIMMUNE CONDITIONS (FIG. 9). Other systemic inflammatory disorders known to cause myocardial fibrosis include rheumatoid arthritis, systemic sclerosis, and systemic lupus erythematosus. In each of these conditions, native T_1 and ECV were noted to be elevated in patients with disease compared with normal controls.[96–98]

IRON DEPOSITION (FIG. 10). Iron overload can be primarily genetic, related to the autosomal recessive condition hemochromatosis, or may be secondary to repeated blood transfusion commonly seen in those with blood or marrow cancers including leukemia, lymphoma, and myeloma or in lifelong transfusion-dependent patients such as those with thalassemia major. Iron normally travels in blood plasma bound to transferrin. When the volume of iron circulating in the body exceeds the transferrin available to bind it and safely store it, it circulates as toxic nontransferrin-bound iron.[99] This nonbound form of iron can be deposited in organs and tissues, including the heart and liver, causing damage at a cellular level. In the heart this can lead to cardiomyopathy. It can be successfully managed with chelation therapy or phlebotomy,

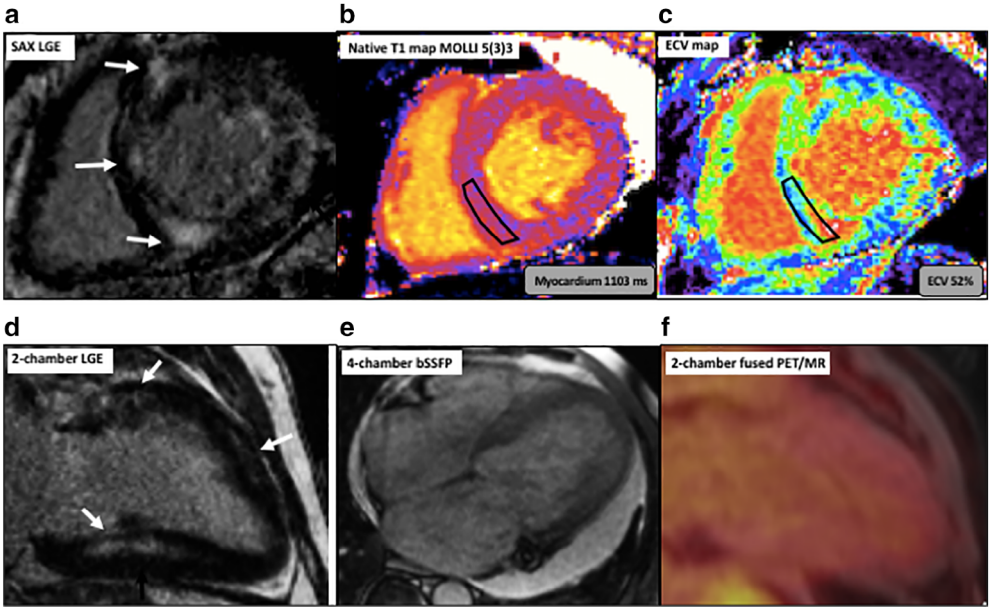

FIGURE 9: Systemic lupus erythematosis. A 50-year-old male patient presented with a past medical history of atrial fibrillation/flutter and lupus nephritis postrenal transplant with new reduction in left ventricular ejection fraction (30%) on echocardiogram. PET/MR was requested for evaluation of cardiomyopathy. a,d: Short axis and two-chamber LGE imaging shows extensive multifocal areas of mesocardial and epicardial delayed enhancement (arrows). b: Native T_1 map demonstrates increased T_1 times. c: Postcontrast T_1 map allows calculation of ECV, which is elevated at 52%. e: CMR also showed a moderate, free-flowing pericardial effusion, possibly related to systemic lupus. f: Two-chamber fused PET/MR image did not show any areas of focal FDG uptake. The combined PET/MR findings suggested that, although there was extensive cardiac infiltrative disease, it was likely long-standing, as it was not metabolically active at the time of imaging.

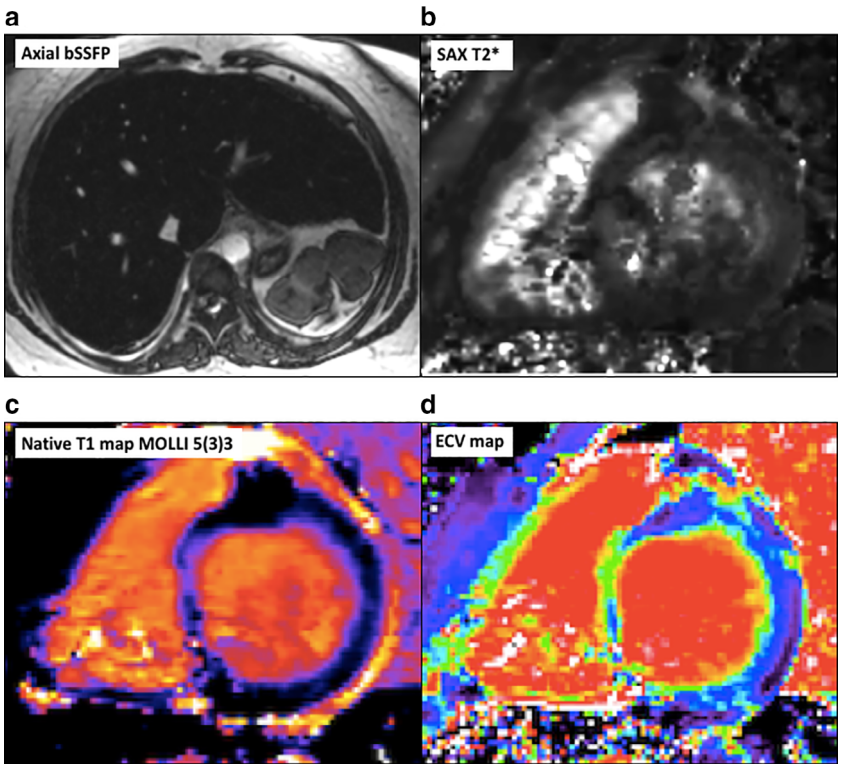

FIGURE 10: Hemochromatosis. A 30-year-old female patient with sickle cell anemia and liver failure secondary to hepatic iron deposition related to numerous blood transfusions. a: Axial bSSFP sequence demonstrates an enlarged liver with diffusely markedly decreased signal compatible with iron deposition. The spleen is also noted to be absent in this image due to auto-splenectomy. b: Short axis T_2* imaging analysis proved severe myocardial iron deposition (T_2* 6 msec, normal range 23–49 msec). c,d: Markedly reduced native T_1 values of 650–700 msec were noted. The ECV was also elevated at 32%, with a hematocrit of 18%.

but treatments work best when the iron deposition is detected at an early stage. Iron is a paramagnetic substance that alters the magnetic field within an MRI magnet. It is known to shorten the T_1, T_2, and T_2* MR signal constants. This property is exploited in T_2* mapping, which allows for detection as well as semiquantitative analysis of iron deposition levels in myocardium.[100] Limitations of the T_2* technique include susceptibility to field inhomogeneities and reduced sensitivity for detection of changes associated with mild or early iron overload. It has been shown that there is a linear relationship between T_1 and T_2* for patients with myocardial iron overload, which suggests that T_1 mapping may also be used for evaluation of iron deposition.[101] That study, in patients with thalassemia major, also suggested that T_1 mapping may allow for better tissue characterization at milder levels of iron deposition, as it is less susceptible to field inhomogeneities. Further supporting this, a study evaluating the use of T_1 mapping in iron overload in patients with a variety of underlying conditions found that myocardial T_1 correlated with T_2* for quantification of iron overload, but was more reproducible and has the potential to detect milder levels of iron deposition.[102]

Similar to myocardial fibrosis, elevated noncontrast liver T_1 values have been used as a noninvasive marker of liver cirrhosis.[103–106] Increased hepatic iron concentration (HIC) is common in this patient population, with shortening of T_1, T_2, and T_2*. As a result, cirrhotic liver T_1 values may pseudo-normalize in the presence of HIC, particularly for MOLLI T_1 measurements due to its sensitivity to T_2 and T_2*. One proposed approach for compensating MOLLI and ShMOLLI T_1 values in the presence of HIC is to use Bloch equation simulations to determine the apparent T_1 value at various combinations of HIC and cirrhosis.[106] A separate T_2* measurement can be used to measure HIC, and the simulation data used as a lookup table to estimate the "compensated T_1" (cT_1) or cirrhosis without the effects of HIC. Saturation recovery techniques have reduced pseudo-normalization due to their independence to T_2, but the effects of T_1 shortening from HIC may still mask the effects of cirrhosis. T_1 measurements using a bSSFP imaging readout common with MOLLI and SASHA may also be significantly affected by steatosis and off-resonance.[107,108] Using a similar Bloch equation simulation model approach of this effect, T_1 measurements at multiple off-resonance frequencies have been used to quantify fat fractions in skeletal muscle.[107] To our knowledge, these iron and fat corrections have not yet been described in relation to cardiac imaging.

ANDERSON–FABRY DISEASE (FIG. 11). Anderson–Fabry disease is a rare X-linked lysosomal storage disorder where a genetic deficiency of the enzyme alpha-galactosidase A results in accumulation of glycosphingolipids within cells. These cause cell abnormalities and organ dysfunction that is particularly manifested in the heart and kidneys. Over time, this excessive intracellular glycosphingolipid results in LV hypertrophy and ultimately fibrosis, which is characteristically seen in the mid-myocardial inferolateral wall.[109] Clinically, this process leads to heart failure and arrhythmias. The intracellular lipid component results in significantly decreased native T_1 values, most marked in those with ventricular hypertrophy but which can be identified even before the LV becomes hypertrophied.[110,111] This suggests that T_1 mapping may be used to identify increased glycosphingolipid storage at an early stage. A potential pitfall with T_1 values in patients with Anderson–Fabry disease is that T_1 values may change over time. The accumulation of glycosphingolipids causes decreased T_1 values compared with normal myocardium, but in the later stage resultant myocardial fibrosis causes increased T_1 values. Segmental analysis of the inferolateral wall demonstrated normal or increased T_1 values in the presence or absence of LGE, and so it is suggested that native T_1 measurements be performed in the interventricular septum in these patients, avoiding areas of LGE.[110] As Anderson–Fabry disease is initially an intracellular disease process before it progresses to the fibrotic stage, ECV is often normal in this patient population.[111]

LIPOMATOUS METAPLASIA. Lipomatous metaplasia refers to deposition of fat in the myocardium and it is associated with reduced native T_1 values in the region of fat deposition. This is most commonly seen postmyocardial infarction but is also seen in arrythmogenic RV dysplasia. Difficulties exist with T_1 mapping in the RV, notably the thinness of the myocardial wall compared with the LV, with increased susceptibility to motion artifact and partial volume averaging. To our knowledge, with the exception of one suspected case of arrythmogenic RV dysplasia (ARVD) included in a cohort of 22 patients with cardiomyopathy but not LGE,[112] native T_1 and ECV values specific to ARVD have not been evaluated.

New Applications of T_1 Mapping

Stress T_1 Mapping

Conventional native T_1 mapping characterizes myocardial diseases by changes in intracellular and interstitial composition and volume, whereas ECV mapping quantifies the ECV volume by changing the relaxation time of the extracellular volume with contrast. A new application of T_1 mapping has been recently described where changes in the myocardial blood volume with stress are used as a surrogate for coronary artery disease. Myocardial T_1 values are measured before and during pharmacological adenosine stress and the change in myocardial T_1 is termed the T_1 reactivity. In healthy myocardium, increased vascular volume results in longer myocardial T_1 values by up to 6% due to the increased volume of long T_1 blood.[113] In obstructive coronary artery disease (CAD), capillary vascular capacity is maximized or near maximized at

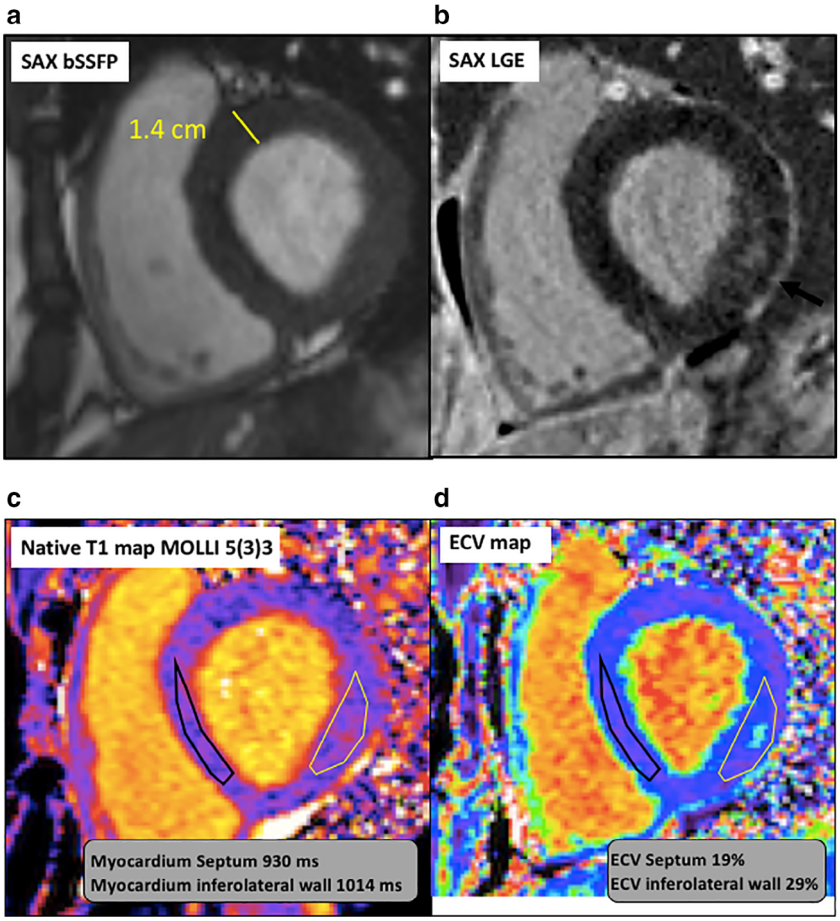

FIGURE 11: Anderson–Fabry disease. A 49-year-old asymptomatic male with a history of Anderson–Fabry disease on Fabryzyme with minimal proteinuria. Mild concentric left ventricular hypertrophy was noted on surveillance echocardiogram. a: Short axis bSSFP image shows mild left ventricular concentric hypertrophy with wall thickness measuring up to 1.4 cm in end-diastole. b: Area of ill-defined gadolinium enhancement in the inferolateral wall (arrow), in a region of typical fibrosis in Anderson–Fabry Disease. c: Native T_1 map demonstrates low values in the background myocardium, sampled here in the inferior septum (white) consistent with glycosphingolipid accumulation. Significantly higher native T_1 values are noted in the region of fibrosis in the inferolateral wall (yellow). d: Postcontrast T_1 maps allow calculation of a reduced ECV (19%) in the background myocardium as sampled in the inferior interventricular septum (white) and significantly higher, borderline increased ECV (29%) in the region of scarring in the inferolateral wall (yellow).

rest and flow does not significantly increase during stress and may actually decrease if blood is shunted elsewhere.

In an initial study in 2014, Mahmod et al found increased native T_1 values and reduced T_1 reactivity with adenosine stress in patients with severe aortic stenosis without obstructive CAD compared with normal controls.[113] These changes normalized when evaluated 7 months postaortic valve replacement, suggesting improved flow reserve. A further proof of concept study in 2016 found up to 6% T_1 reactivity during stress in normal myocardium, but no significant T_1 reactivity in ischemic or infarcted tissues.[114] Furthermore, native T_1 values were higher in ischemic myocardium compared with normal myocardium and were further increased in infarcted myocardium. This study suggests the potential for classification of normal vs. ischemic or infarcted myocardium using a combination of native and stress T_1 mapping without gadolinium contrast. More recent stress T_1 studies have distinguished microvascular dysfunction and epicardial obstructive CAD in native coronary arteries[115] and identified reduced T_1 stress reactivity in patients with well-controlled type 2 diabetes mellitus without obstructive CAD, suggestive of early microvascular changes.[116] Other groups have also employed the technique in small samples but the ability to reliably distinguish between normal, ischemic, and infarcted myocardium remains to be definitively proven.[117–119]

T_1 Mapping in Patients With Implantable Devices / Wideband Arrhythmia Insensitive Rapid (AIR) Pulse Sequences

As we begin to more regularly image patients with implantable devices, including MR-conditional pacemakers and defibrillators, we need to adapt to reduce associated artifacts. The most commonly employed T_1 mapping techniques referenced above, including MOLLI, ShMOLLI, and SASHA, are generally not suitable for use in these patients. Several wideband sequences have been developed to reduce artifact, including

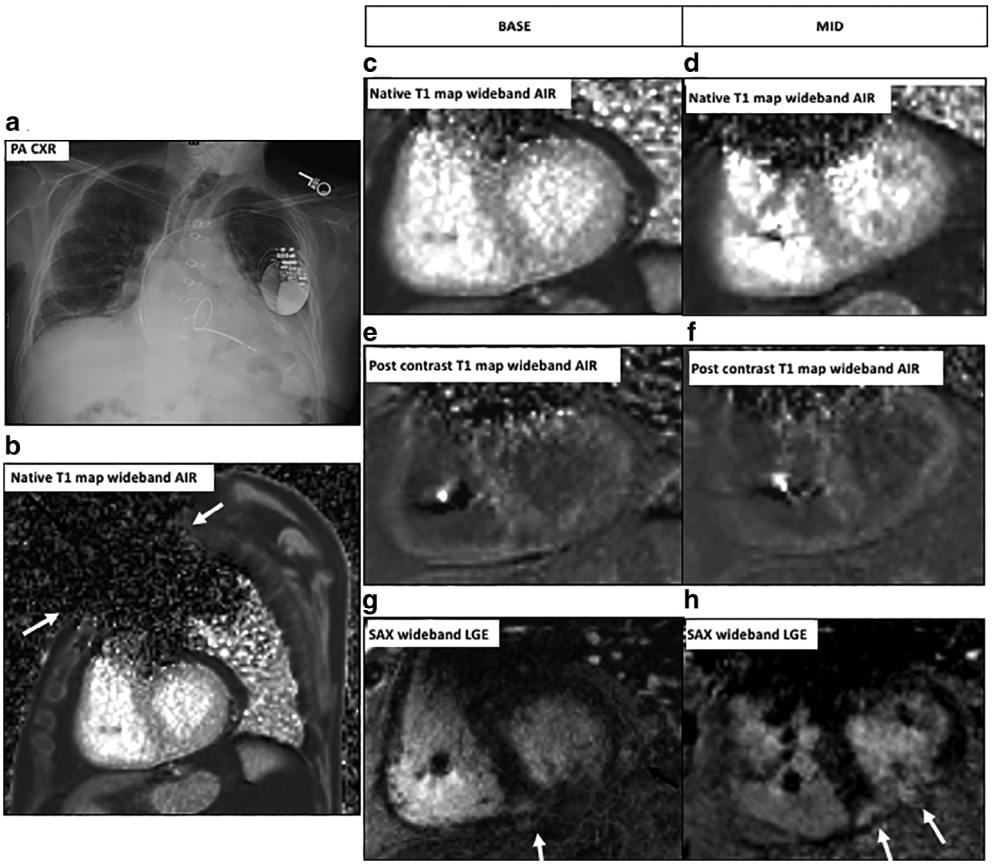

FIGURE 12: Wideband AIR imaging in a patient with scleroderma. A 68-year-old male patient with a prior history of mitral valve repair and proven scleroderma with infiltrative cardiomyopathy with ICD in situ. Left heart catheterization showed very mild coronary artery disease. He presented with increased fatigue and dyspnea on exertion. Echocardiogram showed a newly reduced left ventricular ejection fraction of 15–20%. Cardiac MRI was performed to evaluate extent of scleroderma cardiomyopathy. a: PA chest radiograph demonstrates a single lead ICD in situ. The patient was not pacemaker-dependent and was suitable to proceed with CMR as per departmental protocols. b: Although extensive artifact is seen in the chest wall related to the ICD box (arrows), diagnostic T_1 mapping could be performed of much of the myocardium. c–f: Pre- and postcontrast T_1 maps through the base and mid showed elevated T_1 and calculated ECV values. g,h: Large areas of delayed epicardial and mesocardial enhancement are seen in the corresponding basal and mid segments (arrows).

an AIR sequence incorporating a saturation RF pulse which can produce diagnostic quality images[120] (Fig. 12). Another sequence employing a wideband inversion recovery spoiled gradient echo readout has also been described.[121]

Limitations of T_1 Mapping

Many advances have been made in the field of T_1 mapping over the last two decades, but several factors have limited its translation into widespread clinical practice. One of the most significant limitations is the lack of reference normal ranges of values. Due to differences in accuracy between T_1 mapping techniques and potential sensitivity to protocol parameters, normal values can vary significantly between institutions, as illustrated in a recent large meta-analysis performed by Gottbrecht et al.[122] As a result, it is recommended that each institution establish their own reference values for their particular scanners, T_1 imaging sequence, and contrast protocol. For publications, researchers are encouraged to be transparent and detailed in their descriptions of methods with regard to the exact sequence parameters.

As with all cardiac imaging, potential artifacts should be considered during interpretation of T_1 data. In regions of thin or obliquely oriented myocardium such as the RV and pathologically thinned myocardial walls seen with chronic scarring or dilatation, partial volume averaging with blood or fat can lead to significant errors in both native T_1 values and ECV. At high heart rates, cardiac motion during single-shot imaging can result in blurring of the myocardium and erroneous T_1 values. Motion correction algorithms are commonly used to address residual cardiac or respiratory motion between single-shot images, but incomplete motion correction may also result in apparent T_1 abnormalities. As ECV maps have the further step of motion correction between two different T_1 acquisitions, special care should be taken to check the source T_1-weighted images as part of the interpretation.

The published literature suggests that myocardial T_1 mapping is a useful tool in the diagnostic evaluation and

prognostication of a wide variety of myocardial disorders, as detailed above. However, due to the relatively small changes in T_1 in most diseases, T_1 mapping has limited ability to distinguish between these disorders on its own, and findings should be guided by the clinical condition of the patient, pertinent history, laboratory values, and associated imaging findings.

Native myocardial T_1 values are a single value in each voxel that reflects the composition of the intracellular, intravascular, and interstitial components altogether. As a result, it cannot identify which specific component is abnormal and it is possible that combined disease processes could result in tissue alterations that numerically negate each other within a single voxel, thereby masking the abnormality. This "pseudonormalization" is rare, as most cardiomyopathies increase T_1 values, but has been reported in cases of Fabry disease in combination with diffuse fibrosis (Fig. 11). Nevertheless, it is important to consider the underlying disease process and its potential changes to T_1 values of each compartment during clinical interpretation.

Future Directions

Development of Normal Values

Although diversity in acquisition and postprocessing methodology are intrinsic to the development of any technique, the requirement for scanner-specific normative values must be addressed for widespread clinical application of T_1 mapping. This has led to a push for improved standardization of both the acquisition technique and postprocessing methodology, as highlighted by the most recent consensus statement on CMR mapping techniques from the Society for Cardiovascular Magnetic Resonance (SCMR), which was endorsed by the European Association for Cardiovascular Imaging (EACVI).[30] Standardized accuracy and precision validation using phantoms such as T1MES[123] provide reproducible methods for comparing both acquisition and postprocessing workflows. Single-center and small-scale multicenter studies have started to establish normal values for various techniques and pathologies,[14,36–40,124–127] but significant work remains for these studies to be widely adopted.

Acquisition Technique Development

At the same time, techniques for parametric mapping continue to improve. Recent advances in pulse sequence modeling and image reconstruction have led to the development of computational approaches to parametric mapping. Conventional T_1 mapping acquires images at multiple times following an inversion or saturation recovery preparation, and exponential curve fitting is used to calculate a T_1 value. Cardiac MR fingerprinting is an alternative approach where highly undersampled spiral acquisitions are acquired following T_1 or T_2 preparation pulses.[128] The magnetization evolution during the acquisition is characteristic of a specific combination of T_1 and T_2, and thus the T_1 and T_2 values can be simultaneously determined by pattern matching. CMR multitasking is another computational approach to parametric mapping, where continuous golden-angle radial data are acquired following an inversion pulse without ECG gating or breath-holding.[129] Low-rank tensor modeling is used to resolve both cardiac and respiratory motion during reconstruction, yielding dynamic T_1 maps as a function of cardiac or respiratory phase. These techniques have the potential for faster and easier to use multiparametric mapping, but are still in active development and require validation in a larger multicenter studies.

Machine Learning

As with many other fields of medical imaging, there is significant interest in the application of machine learning to T_1 mapping. Such techniques have already been applied to CMR image analysis, where it has been used for segmentation of cine images and automatic calculation of functional and anatomical parameters, including ejection fraction and myocardial mass. Similarly, a fully convolutional neural network has been proposed for the automated segmentation of native T_1 maps, potentially offering a faster and less operator-dependent workflow.[130]

Machine learning can also be used to automate the analysis of spatial variations in T_1 over the myocardium. This approach, termed texture analysis, is a fairly novel method of evaluating medical images to detect patterns associated with diseased tissues that are not always detectable by the human eye. One study involving T_1 maps of 50 subjects with dilated cardiomyopathy and 24 healthy controls found that 9 of 12 histogram parameters were significantly different in patients with DCM compared with healthy controls. Gray-level patterns entropy, contrast, and homogeneity were also significantly different between the two groups.[131] Another study was performed involving 39 patients with infarct-like myocarditis and 10 healthy controls including both T_1 and T_2 maps.[132] Using a Boruta texture feature selection process, 29 of 31 T_1 mapping features were found to be non-important and excluded from the analysis. Of the two T_1 texture features chosen for analysis, only one (T_1 sigma) showed a significant difference between the patients and controls, but its performance as a single parameter was inferior to the four T_2 texture features chosen for analysis. The mixed results from these initial investigations warrant further study to determine the potential usefulness of texture analysis of T_1 mapping data.

Conclusion

Native T_1 mapping and ECV are promising advanced CMR imaging techniques with demonstrated clinical applications to a variety of cardiac conditions. In particular, native T_1

mapping is very valuable in that administration of contrast is not required, which is desirable for the patient and for streamlining the acquisition process. Research is currently ongoing in order to improve speed and precision of acquisition techniques and to standardize reference values in order to integrate this technique into routine clinical care.

Acknowledgment

We thank Ryan Avery, MD, for providing fused PET/MR image Figure 9F.

References

1. Kim RJ, Fieno DS, Parrish TB, et al. Relationship of MRI delayed contrast enhancement to irreversible injury, infarct age, and contractile function. Circulation 1999;100:1992–2002.
2. Ferreira PF, Gatehouse PD, Mohiaddin RH, Firmin DN. Cardiovascular magnetic resonance artefacts. J Cardiovasc Magn Reson 2013;15:41.
3. Look DC, Locker DR. Time saving in measurement of NMR and EPR relaxation times. Rev Sci Instrum 1970;41:250–251.
4. Deichmann R, Haase A. Quantification of T1 values by Snapshot-FLASH NMR imaging. J Magn Reson 1992;96:608–612.
5. Gai N, Turkbey EB, Nazarian S, et al. T1 mapping of the gadolinium-enhanced myocardium: Adjustment for factors affecting interpatient comparison. Magn Reson Med 2011;65:1407–1415.
6. Nacif MS, Turkbey EB, Gai N, et al. Myocardial T1 mapping with MRI: Comparison of Look-Locker and MOLLI sequences. J Magn Reson Imaging 2011;34:1367–1373.
7. Messroghli DR, Radjenovic A, Kozerke S, Higgins DM, Sivananthan MU, Ridgway JP. Modified Look-Locker inversion recovery (MOLLI) for high resolution T1 mapping of the heart. Magn Reson Med 2004;52:141–146.
8. Kellman P, Hansen MS. T1-mapping in the heart: Accuracy and precision. J Cardiovasc Magn Reson 2014;16:2.
9. Messroghli DR, Greiser A, Frohlich M, Dietz R, Schulz-Menger J. Optimization and validation of a fully integrated pulse sequence for modified Look-Locker inversion recovery (MOLLI) T1 mapping of the heart. J Magn Reson Imaging 2007;26:1081–1086.
10. Gai ND, Stehning C, Nacif M, Bluemke DA. Modified Look-Locker T (1) evaluation using Bloch simulations: Human and phantom validation. Magn Reson Med 2013;69 :329–336.
11. Robson MD, Piechnik SK, Tunnicliffe EM, Neubauer S. T1 measurements in the human myocardium: The effects of magnetization transfer on the SASHA and MOLLI sequences. Magn Reson Med 2013; 670:664–670.
12. Kellman P, Herzka DA, Arai AE, Hansen MS. Influence of off-resonance in myocardial T1-mapping using SSFP based MOLLI method. J Cardiovasc Magn Reson 2013;15:63.
13. Kellman P, Herzka DA, Hansen MS. Adiabatic inversion pulses for myocardial T1 mapping. Magn Reson Med 2014;71:1428–1434.
14. Piechnik SK, Ferreira VM, Dall'Armellina E, et al. Shortened Modified Look-Locker Inversion recovery (ShMOLLI) for clinical myocardial T1-mapping at 1.5 and 3 T within a 9 heartbeat breathhold. J Cardiovasc Magn Reson 2010;12:69.
15. Chow K, Flewitt JA, Green JD, Pagano JJ, Friedrich MG, Thompson RB. Saturation recovery single-shot acquisition (SASHA) for myocardial T(1) mapping. Magn Reson Med 2013;70:1274–1282.
16. Slavin GS, Hood MN, Ho VB, Stainsby JA. Breath-held myocardial T1 mapping using multiple single-point saturation recovery. In: Proc 20th Annual Meeting ISMRM, Melbourne; 2012. p 1244.
17. Higgins DM, Ridgway JP, Radjenovic A, Sivananthan UM, Smith MA. T1 measurement using a short acquisition period for quantitative cardiac applications. Med Phys 2005;32:1738–1746.
18. Wacker CM, Bock M, Hartlep AW, et al. Changes in myocardial oxygenation and perfusion under pharmacological stress with dipyridamole: Assessment using T*2 and T1 measurements. Magn Reson Med 1999;41:686–695.
19. Roujol S, Weingartner S, Foppa M, et al. Accuracy, precision and reproducibility of four T1 mapping sequences: A head to head comparison of MOLLI, ShMOLLI, SASHA and SAPPHIRE. Radiology 2014; 272:683–689.
20. Chow K, Flewitt J, Pagano JJ, Green JD, Friedrich MG, Thompson RB. T2-dependent errors in MOLLI T1 values: Simulations, phantoms, and in-vivo studies. J Cardiovasc Magn Reson 2012;14 (Suppl 1):P281.
21. Chow K, Spottiswoode BS, Pagano JJ, Thompson RB. Improved precision in SASHA T1 mapping with a variable flip angle readout. J Cardiovasc Magn Reson 2014;16(Suppl 1):M9.
22. Kellman P, Xue H, Chow K, Spottiswoode BS, Arai AE, Thompson RB. Optimized saturation recovery protocols for T1-mapping in the heart: Influence of sampling strategies on precision. J Cardiovasc Magn Reson 2014;16:55.
23. Chow K, Flewitt JA, Sandonato R, et al. Reproducibility and performance of SASHA and MOLLI T1 mapping in volunteers at 1.5T and 3T. In: Proc SCMR 2018 Conference. p 863.
24. Weingärtner S, Akçakaya M, Basha T, et al. Combined saturation/inversion recovery sequences for improved evaluation of scar and diffuse fibrosis in patients with arrhythmia or heart rate variability. Magn Reson Med 2014;71:1024–1034.
25. Guo R, Chen Z, Wang Y, Herzka DA, Luo J, Ding H. Three-dimensional free breathing whole heart cardiovascular magnetic resonance T1 mapping at 3 T. J Cardiovasc Magn Reson 2018;20:64.
26. Chen Y, Lo WC, Hamilton JI, et al. Single breath-hold 3D cardiac T1 mapping using through-time spiral GRAPPA. NMR Biomed 2018;31: e3923.
27. Nordio G, Henningsson M, Chiribiri A, Villa ADM, Schneider T, Botnar RM. 3D myocardial T1 mapping using saturation recovery. J Magn Reson Imaging 2017;46:218–227.
28. Chow K, Yang Y, Shaw P, Kramer CM, Salerno M. Robust free-breathing SASHA T1 mapping with high-contrast image registration. J Cardiovasc Magn Reson 2016;18:47.
29. Moon JC, Messroghli DR, Kellman P, et al. Myocardial T1 mapping and extracellular volume quantification: A Society for Cardiovascular Magnetic Resonance (SCMR) and CMR Working Group of the European Society of Cardiology Consensus Statement. J Cardiovasc Magn Reson 2013;15:92.
30. Messroghli DR, Moon JC, Ferreira VM, et al. Clinical recommendations for cardiovascular magnetic resonance mapping of T1, T2, T2* and extracellular volume: A consensus statement by the Society of Cardiovascular Magnetic Resonance (SCMR) endorsed by the European Association for Cardiovascular Imaging (EACVI). J Cardiovasc Magn Reson 2017;19:75.
31. Schelbert EB, Testa SM, Meier CG, et al. Myocardial extravascular volume fraction measurement by gadolinium cardiovascular magnetic resonance in humans: Slow infusion versus bolus. J Cardiovasc Magn Reson 2011;13:16.
32. Kawel N, Nacif M, Zavodni A, et al. T1 mapping of the myocardium intra-individual assessment of the effect of field strength, cardiac cycle and variation by myocardial region. J Cardiovasc Magn Reson 2012; 14:27.
33. Flett AS, Hayward MP, Ashworth MT, et al. Equilibrium contrast cardiovascular magnetic resonance for the measurement of diffuse myocardial fibrosis: Preliminary validation in humans. Circulation 2010; 122:138–144.
34. Miller CA, Naish J, Bishop P, et al. Comprehensive validation of cardiovascular magnetic resonance techniques for the assessment of

myocardial extracellular volume. Circ Cardiovasc Imaging 2013;6: 373–383.

35. Treibel TA, Fontana M, Maestrini V, et al. Automatic measurement of the myocardial interstitium: Synthetic extracellular volume quantification without hematocrit sampling. J Am Coll Cardiol Imaging 2016;9: 54–63.

36. Dabir D, Child N, Kalra A, et al. Reference values for healthy human myocardium using a T1 mapping methodology: Results from the International T1 Multicenter Cardiovascular Magnetic Resonance Study. J Cardiovasc Magn Reson 2014;16:69.

37. Rauhalammi SM, Mangion K, Barrientos PH, et al. Native myocardial longitudinal (T1) relaxation time: Regional, age, and sex associations in the healthy adult heart. J Magn Reson Imaging 2016;44:541–548.

38. Rosimini S, Bulluck H, Captur G, et al. Myocardial native T1 and extracellular volume with healthy aging and gender. Eur Heart J Cardiovasc Imaging 2019;9:615–621.

39. Bulluck H, Bryant JA, Tan JZ, et al. Gender differences in native myocardial T1 in a healthy Chinese volunteer cohort. Cardiovasc Imaging Asia 2017;1:110–115.

40. Costello BT, Springer F, Hare JL, et al. SASHA versus ShMOLLI: A comparison of T1 mapping methods in health and dilated cardiomyopathy at 3T. Int J Cardiovasc Imaging 2017;33:1551–1560.

41. Kellman P, Arai AE, Xue H. T1 and extracellular volume mapping in the heart: Estimation of error maps and the estimation of noise on precision. J Cardiovasc Magn Reson 2013;15:56.

42. Piechnik SK, Ferreira VM, Lewandowski AJ, et al. Normal variation of magnetic resonance T1 relaxation times in the human population at 1.5 T using ShMOLLI. J Cardiovasc Magn Reson 2013;15:13.

43. Fontana M, White SK, Banypersad SM, et al. Comparison of T1 mapping techniques for ECV quantification. Histological validation and reproducibility of ShMOLLI versus multi-breath-hold T1 quantification equilibrium contrast CMR. J Cardiovasc Magn Reson 2012;14:88.

44. Liu CY, Bluemke DA, Gerstenblith G, et al. Reference values of myocardial structure, function and tissue composition by cardiac magnetic resonance in healthy African-Americans at 3T and their relations to serologic and cardiovascular risk factors. Am J Cardiol 2014;114: 789–795.

45. Liu CY, Liu YC, Wu C, et al. Evaluation of age-related interstitial myocardial fibrosis with cardiac magnetic resonance contrast-enhanced T1 mapping: MESA (Multi-Ethnic Study of Atherosclerosis). J Am Coll Cardiol 2013;62:1280–1287.

46. von Knobelsdorff-Brenkenhoff F, Prothmann M, Dieringer MA, et al. Myocardial T1 and T2 mapping at 3 T: Reference values, influencing factors and implications. J Cardiovasc Magn Reson 2013;15:53.

47. Ferreira VM, Piechnik SK, Dall'Armellina E, et al. T(1) mapping for the diagnosis of acute myocarditis using CMR: Comparison to T2-weighted and late gadolinium enhanced imaging. JACC Cardiovasc Imaging 2013;6:1048–1058.

48. Hinojar R, Foote L, Arroyo Ucar E, et al. Native T1 in discrimination of acute and convalescent stages in patients with clinical diagnosis of myocarditis: A proposed diagnostic algorithm using CMR. JACC Cardiovasc Imaging 2015;8:37–46.

49. Radunski UK, Lund GK, Stehning C, et al. CMR in patients with severe myocarditis: Diagnostic value of quantitative tissue markers including extracellular volume imaging. JACC Cardiovasc Imaging 2014;7: 667–675.

50. Verhaert D, Thavendiranathan P, Giri S, et al. Direct T2 quantification of myocardial edema in acute ischemic injury. JACC Cardiovasc Imaging 2011;4:269–278.

51. Ferreira VM, Piechnik SK, Dall'Armellina E, et al. Non-contrast T1-mapping detects acute myocardial edema with high diagnostic accuracy: A comparison to T2-weighted cardiovascular magnetic resonance. J Cardiovasc Magn Reson 2012;14:42.

52. Yu J, Guensch DP, Fischer K, Nadeshalingham G, Friedrich MG. Performance of T1 mapping vs. T2 mapping for assessing myocardial edema. J Cardiovasc Magn Reson 2014;16(Suppl 1):O16.

53. Caforio AL, Pankuweit S, Arbustini E, et al. European Society of Cardiology Working Group on Myocardial and Pericardial Diseases. Current state of knowledge on aetiology, diagnosis, management, and therapy of myocarditis: A position statement of the European Society of Cardiology Working Group on Myocardial and Pericardial Diseases. Eur Heart J 2013;34:2636–2648.

54. Kindermann I, Barth C, Mahfoud F, et al. Update on myocarditis. J Am Coll Cardiol 2012;59:779–792.

55. Lurz P, Luecke C, Eitel I, et al. Comprehensive cardiac magnetic resonance imaging in patients with suspected myocarditis: The MyoRacer-Trial. J Am Coll Cardiol 2016;67:1800–1811.

56. Kinderman I, Kinderman M, Kandolf R, et al. Predictors of outcome in patients with suspected myocarditis. Circulation 2008;118:639–648.

57. Cooper LT, Baughman KL, Feldman AM, et al. The role of endomyocardial biopsy in the management of cardiovascular disease: A scientific statement from the American Heart Association, the American College of Cardiology, and the European Society of Cardiology. Circulation 2007;116:2216–2233.

58. Lurz P, Eitel I, Adam J, et al. Diagnostic performance of CMR imaging compared with EMB in patients with suspected myocarditis. JACC Cardiovasc Imaging 2012;5:513–524.

59. Friedrich MG, Sechtem U, Schulz-Menger J, et al. Cardiovascular magnetic resonance in myocarditis: A JACC white paper. JACC 2009; 53:1475–1487.

60. Bohnen S, Radunski UK, Lund GK, et al. Tissue characterization by T1 and T2 mapping cardiovascular magnetic resonance imaging to monitor myocardial inflammation in healing myocarditis. Eur Heart J Cardiovasc Imaging 2017;18:744–751.

61. Luetkens JA, Doerner J, Thomas DK, et al. Acute myocarditis: Multiparametric cardiac MR imaging. Radiology 2014;273:383–392.

62. Ferreira VM, Schulz-Menger J, Holmvang G, et al. Cardiovascular magnetic resonance in nonischemic myocardial inflammation: Expert Recommendations. JACC 2018;72:3158–3176.

63. Abdel-Aty H, Cocker M, Meek C, Tyberg JV, Friedrich MG. Edema as a very early marker for acute myocardial ischemia: A cardiovascular magnetic resonance study. J Am Coll Cardiol 2009;53:1194–1201.

64. Messroghli DR, Walters K, Plein S, Friedrich MG, Ridgway JP, Sivanantha MU. Myocardial T1 mapping: Application to patients with acute and chronic myocardial infarction. Magn Reson Med 2007;58: 34–40.

65. Dastidar AG, Harries I, Pontecorboli G, et al. Native T1 mapping to detect extent of acute and chronic myocardial infarction: Comparison with late gadolinium enhancement technique. Int J Cardiovasc Imaging 2018 [Epub ahead of print] doi: https://doi.org/10.1007/s10554-018-1467-1.

66. Scally C, Rudd A, Mezincescu A, et al. Persistent long-term structural, functional and metabolic changes after stress induced (Takotsubo) cardiomyopathy. Circulation 2018;137:1039–1048.

67. Chambers DC, Cherikh WS, Goldfarb SB, et al. The International Thoracic Organ Transplant Registry of the International Society for Heart-lung Transplantation: Thirty-fifth adult lung and heart-lung transplant report 2018. J Heart Lung Transplant 2018;37:1169–1183.

68. Vermes E, Pantaleaon C, Pucheux J, Mirza A, Delhommais A, Sirinelli A. Diagnostic value of quantitative tissue markers (T2 mapping and ECV) for acute cardiac rejection diagnosis: A preliminary experience. J Heart Lung Transpl 2014;35:S193.

69. Dolan RS, Rahsepar AA, *Blaisdell J, et al*. Multiparametric cardiac magnetic resonance imaging can detect acute cardiac allograft rejection after heart transplantation. JACC Cardiovasc Imaging 2019 [Epub ahead of print] doi: https://doi.org/10.1016/j.jcmg.2019.01.026.

70. Mewton N, Liu CY, Croisille P, Bluemke D, Lima JA. Assessment of myocardial fibrosis with cardiac magnetic resonance. J Am Coll Cardiol 2011;57:891–903.

71. Weber KT, Sun Y, Bhattacharya SK, Ahokas RA, Gerling IC. Myofibroblast-mediated mechanisms of pathological remodelling of the heart. Nat Rev Cardiol 2013;10:15–26.

72. Kuruvilla S, Adenaw N, Katwal AB, Lipinski MJ, Kramer CM, Salerno M. Late gadolinium enhancement on CMR predicts adverse cardiovascular outcomes in non-ischemic cardiomyopathy: A systematic review and meta-analysis. Circ Cardiovasc Imaging 2014;7: 250–258.

73. Puntmann VO, Voigt T, Chen Z, et al. Native T1 mapping in differentiation of normal myocardium from diffuse disease in hypertrophic and dilated cardiomyopathy. JACC Cardiovasc Imaging 2013;6:475–484.

74. aus dem Siepen F, Buss SJ, Messroghli D, et al. T1 mapping in dilated cardiomyopathy with cardiac magnetic resonance: Quantification of diffuse myocardial fibrosis and comparison with endomyocardial biopsy. Eur Heart J Cardiovasc Imaging 2015;16:210–216.

75. Puntmann VO, Carr-White G, Jabbour A, et al. T1-mapping and outcome in nonischemic cardiomyopathy: All-cause mortality and heart failure. International T1 Multicentre CMR Outcome Study. JACC Cardiovasc Imaging 2016;9:40–50.

76. Youn JC, Hong YJ, Lee HJ, et al. Contrast-enhanced T1 mapping-based extracellular volume fraction independently predicts clinical outcome in patients with non-ischemic dilated cardiomyopathy: A prospective cohort study. Eur Radiol 2017;27:3924–3933.

77. Klues HG, Schiffers A, Maron BJ. Phenotypic spectrum and patterns of left ventricular hypertrophy in hypertrophic cardiomyopathy: Morphologic observations and significance as assessed by two-dimensional echocardiography in 600 patients. J Am Coll Cardiol 1995;26:1699–1708.

78. Davies MJ, McKenna WJ. Hypertrophic cardiomyopathy—Pathology and pathogenesis. Histopathology 1995;26:493–500.

79. Maron MS, Maron BJ, Harrigan C, et al. Hypertrophic cardiomyopathy phenotype revisited after 50 years with cardiovascular magnetic resonance. J Am Coll Cardiol 2009;54:220–228.

80. Dass S, Suttie JJ, Piechnik SK, et al. Myocardial tissue characterization using magnetic resonance non-contrast T1 mapping in hypertrophic and dilated cardiomyopathy. Circ Cardiovasc Imaging 2012;5: 726–733.

81. Hinojar R, Varma N, Child N, et al. T1 mapping in discrimination of hypertrophic phenotypes: Hypertensive heart disease and hypertrophic cardiomyopathy: Findings from the International T1 Multicenter Cardiovascular Magnetic Resonance Study. Circ Cardiovasc Imaging 2015;8.

82. Swoboda PP, McDiarmid AK, Erhayiem B, et al. Assessing myocardial extracellular volume by T1 mapping to distinguish hypertrophic cardiomyopathy from athlete's heart. J Am Coll Cardiol 2016;67: 2189–2190.

83. Towbin JA, Lorts A, Jeffries JL. Left ventricular non-compaction cardiomyopathy. Lancet 2015;386:813–825.

84. Zhou H, Lin X, Fang L, et al. Characterization of compacted myocardial abnormalities by cardiac magnetic resonance with native T1 mapping in Left ventricular non compaction patients: A comparison with late gadolinium enhancement. Circ J 2016;80:1210–1216.

85. Owan TE, Hodge DO, Herges RM, Jacobsen S, Roger VL, Redfield MM. Trends in prevalence and outcome of heart failure with preserved ejection fraction. N Engl J Med 2006;355:251–259.

86. Zile MR, Baicu CF, Gaasch WH. Diastolic heart failure—Abnormalities in active relaxation and passive stiffness of the left ventricle. N Engl J Med 2004;350:1953–1959.

87. Westermann D, Kasner M, Steendijk P, et al. Role of left ventricular stiffness in heart failure with normal ejection fraction. Circulation 2008; 117:2051–2060.

88. Paulus WJ, Tschöpe C. A novel paradigm for heart failure with preserved ejection fraction: Comorbidities drive myocardial dysfunction and remodeling through coronary microvascular endothelial inflammation. J Am Coll Cardiol 2013;62:263–271.

89. Su MM, Lin L, Tseng YE, et al. CMR-verified diffuse myocardial fibrosis is associated with diastolic dysfunction in HFpEF. JACC Cardiovasc Imaging 2014;7:991–997.

90. Maceira AM, Joshi J, Prasad SK, et al. Cardiovascular magnetic resonance in cardiac amyloidosis. Circulation 2005;111:186–193.

91. White JA, Kim HW, Shah D, et al. CMR imaging with rapid visual T1 assessment predicts mortality in patients suspected of cardiac amyloidosis. J Am Coll Cardiol Imaging 2014;7:143–156.

92. Karamitsos TD, Piechnik, Banypersad SM, et al. Noncontrast T1 mapping for the diagnosis of cardiac amyloidosis. JACC Cardiovasc Imaging 2013;6:488–497.

93. Fontana M, Banypersad SM, Treibel TA, et al. Native T1 mapping in transthyretin amyloidosis. JACC Cardiovasc Imaging 2014;7:157–165.

94. Matsui Y, Iwai K, Tachibana T, et al. Clinicopathological study of fatal myocardial sarcoidosis. Ann N Y Acad Sci 1976;278:455–469.

95. Puntmann VO, Isted A, Hinojar R, Foote L, Carr-White G, Nagel E. T1 and T2 mapping in recognition of early cardiac involvement in systemic sarcoidosis. Radiology 2017;285:63–72.

96. Ntusi NAB, Piechnik SK, Francis JM, et al. Diffuse myocardial fibrosis and inflammation in rheumatoid arthritis: Insights from CMR T1 mapping. JACC Cardiovasc Imaging 2015;8:526–536

97. Ntusi NA, Piechnik SK, Francis JM, et al. Subclinical myocardial inflammation and diffuse fibrosis are common in systemic sclerosis—A clinical study using myocardial T1-mapping and extracellular volume quantification. J Cardiovasc Magn Reson 2014;16:21.

98. Puntmann VO, D'Cruz D, Smith Z, et al. Native myocardial T1 mapping by cardiovascular magnetic resonance imaging in subclinical cardiomyopathy in patients with systemic lupus erythematosus. Circ Cardiovasc Imaging 2013;6:295–301.

99. Breuer W, Hershko C, Cabantchik ZI. The importance of non-transferrin bound iron in disorders of iron metabolism. Transfus Sci 2000;23:185–192.

100. Anderson IJ, Holden S, Davis B, et al. Cardiovascular T2-star (T2*) magnetic resonance for the early diagnosis of myocardial iron overload. Eur Heart J 2001;22:2171–2179.

101. Feng Y, He T, Carpenter JP, et al. In vivo comparison of myocardial T1 with T2 and T2* in thalassaemia major. J Magn Reson Imaging 2013;38:588–593.

102. Sado DM, Maestrini V, Piechnik SK, et al. Noncontrast myocardial T1 mapping using cardiovascular magnetic resonance for iron overload. J Magn Reson Imaging 2015;41:1505–1511.

103. Thomsen C, Christofferson P, Henriksen O, Juhl E. Prolonged T1 in patients with liver cirrhosis: An in vivo MRI study. Magn Reson Imaging 1990;8:599–604.

104. Hoad CL, Palaniyappan N, Kaye P, et al. A study of T1 relaxation time as a measure of liver fibrosis and influence of confounding histological factors. NMR Biomed 2015;28:706–714.

105. Banerjee R, Pavlides M, Tunnicliffe EM, et al. Multiparametric magnetic resonance for the non-invasive diagnosis of liver disease. J Hepatol 2014;60:69–77.

106. Tunnicliffe EM, Banerjee R, Pavlides M, Neubauer S, Robson MD. A model for hepatic fibrosis: The competing effects of cell loss and iron on shortened modified Look-Locker inversion recovery T1 (shMOLLI-T1) in the liver. J Magn Reson Imaging 2017;45:450–462.

107. Larmour S, Chow K, Kellman P, Thompson RB. Characterization of T1 bias in skeletal muscle from fat in MOLLI and SASHA pulse sequences: Quantitative fat-fraction imaging with T1 mapping. Magn Reson Med 2017;77:237–249.

108. Kellman P, Bandettini WP, Mancini C, Hammer-Hansen S, Hansen MS, Arai AE. Characterization of myocardial T1-maping bias caused by intramyocardial fat in inversion recovery and saturation recovery techniques. J Cardiovasc Magn Reson 2015;17:33.

109. Moon JCC, Sachdev B, Elkington AG, et al. Gadolinium enhanced cardiovascular magnetic resonance in Anderson-Fabry disease. Evidence for a disease specific abnormality of the myocardial interstitium. Eur Heart J 2003;24:2151–2155.

110. Sado DM, White SK, Piechnik SK, et al. Identification and assessment of Anderson-Fabry disease by cardiovascular magnetic resonance

noncontrast myocardial T1 mapping. Circ Cardiovasc Imaging 2013;6: 392–398.

111. Thompson RB, Chow K, Khan A, et al. T1 mapping with cardiovascular MRI is highly sensitive for Fabry disease independent of hypertrophy and sex. Circ Cardiovasc Imaging 2013;6:637–645.

112. Sibley CT, Noureldin RA, Gai N, et al. T1 mapping in cardiomyopathy at cardiac MR: Comparison with endomyocardial biopsy. Radiology 2012;25:74–732.

113. Mahmod M, Piechnik SK, Levelt E, et al. Adenosine stress native T1 mapping in severe aortic stenosis: Evidence for a role of the intravascular compartment on myocardial T1 values. J Cardiovasc Magn Reson 2014;16:92.

114. Liu A, Wijesurendra RS, Francis JM, et al. Adenosine stress and rest T1 mapping can differentiate between ischemic, infarcted, remote and normal myocardium without the need for gadolinium contrast agents. JACC Cardiovasc Imaging 2016;9:27–36.

115. Liu A, Wijesurendra RS, Liu JM, et al. Gadolinium-free cardiac MR stress T1-mapping to distinguish epicardial from microvascular coronary disease. JACC 2018;71:957–968.

116. Levelt E, Piechnik SK, Liu A, et al. Adenosine stress CMR T1-mapping detects early microvascular dysfunction in patients with type 2 diabetes mellitus without obstructive coronary artery disease. J Cardiovasc Magn Reson 2017;19:81.

117. Bohnen S, Prussner L, Vettorazzi E, et al. Stress T1-mapping cardiovascular magnetic resonance imaging and inducible myocardial ischemia. Clin Res Cardiol 2019 [Epub ahead of print] doi:https://doi.org/10.1007/s00392-019-01421-1.

118. Kuijpers D, Prakken NH, Vliegenthart R, van Dijkman PRM, van der Harst P, Oudkerk M. Caffeine intake inverts the effect of adenosine on myocardial perfusion during stress as measured by T1 mapping. Int J Cardiovasc Imaging 2016;32:1545–1553.

119. Nakamori S, Fahmy A, Jang J, et al. Changes in myocardial T1 and T2 after supine exercise stress in healthy and ischemic myocardium: A pilot study. Circulation 2018;138:A15014.

120. Hong K, Jeong EK, Wall TS, Drakos SG, Kim D. Wideband arrhythmia-insensitive-rapid (AIR) pulse sequence for cardiac T1 mapping without image artifacts induced by an implantable-cardioverter-defibrillator. Magn Reson Med 2015;74:336–345.

121. Shao J, Rashid S, Renella P, Nguyen KL, Hu P. Myocardial T1 mapping for patients with implanted cardiac devices using wideband inversion recovery spoiled gradient echo readout. Magn Reson Med 2017;77:1495–1504.

122. Gottbrecht M, Kramer CM, Salerno M. Native T1 and extracellular volume measurements by cardiac MRI in healthy adults: A meta-analysis. Radiology 2019;290:317–326.

123. Captur G, Gatehouse P, Keenan KE, et al. A medical device-grade T1 and ECV phantom for global T1 mapping quality assurance-the T1 Mapping and ECV Standardization in cardiovascular magnetic resonance (T1MES) program. J Cardiovasc Magn Reson 2016;18:58.

124. Roy C, Slimani A, de Meester C, et al. Age and sex corrected normal reference values of T1, T2, T2* and ECV in healthy subjects at 3T CMR. J Cardiovasc Magn Reson 2017;19:72.

125. Liu JM, Liu A, Leal J, et al. Measurement of myocardial native T1 in cardiovascular diseases and nom in 1291 subjects. J Cardiovasc Magn Reson 2017;19:74.

126. Gottbrecht M, Kramer CM, Salnero M. Native T1 and extracellular volume measurements by cardiac MRI in healthy adults: A meta-analysis. Radiology 2019;290:317–326.

127. Pagano JJ, Chow K, Paterson DI, et al. Effects of age, gender and risk factors for heart failure on native myocardial T1 and extracellular volume fraction using the SASHA sequence at 1.5T. J Magn Reson Imaging 2018;47:1307–1317.

128. Hamilton JI, Jiang Y, Chen Y, et al. MR fingerprinting for rapid quantification of myocardial T1, T2, and proton spin density. Magn Reson Med 2017;77:1446–1458.

129. Shaw JL, Yang Q, Zhou Z, et al. Free-breathing, non-ECG, continuous myocardial T1 mapping with cardiovascular magnetic resonance multitasking. Magn Reson Med 2019;81:2450–2463.

130. Fahmy AS, El-Rewaidy H, Nezafat M, Nakamori S, Nezafat R. Automated analysis of cardiovascular magnetic resonance myocardial native T1 mapping images using fully convolutional neural networks. J Cardiovasc Magn Reson 2019;21:7.

131. Xiao-Ning S, Ying-Jie S, Kun-Tao, X, et al. Texture analysis of magnetic resonance T1 mapping with dilated cardiomyopathy: A machine learning approach. Medicine 2018;97:e12246.

132. Baessler B, Luecke C, Lurz J, et al. Cardiac MRI texture analysis of T1 and T2 maps in patients with infarctlike acute myocarditis. Radiology 2018;289:357–365.